Transcriptional profiling reveals TRPM5-expressing cells involved in viral infection in the olfactory epithelium

B. Dnate' Baxter[1,2,‡], Eric D. Larson[3 ‡], Paul Feinstein[4], Arianna Gentile Polese[1,2], Andrew N. Bubak[5], Christy S. Niemeyer[5], James Hassell, Jr.[5], Laetitia Merle[1,2], Doug Shepherd[6], Vijay R. Ramakrishnan[3], Maria A. Nagel[5], and Diego Restrepo[1,2,*]

[1]Neuroscience Graduate Program, University of Colorado Anschutz Medical Campus, Aurora, CO 80045, USA

[2]Department of Cell and Developmental Biology, University of Colorado Anschutz Medical Campus, Aurora, CO 80045, USA

[3]Department of Otolaryngology, University of Colorado Anschutz Medical Campus, Aurora, CO 80045, USA

[4]Department of Biological Sciences, Hunter College, CUNY, New York, NY, 10065, USA

[5]Department of Neurology, University of Colorado Anschutz Medical Campus, Aurora, CO 80045, USA

[6]Department of Pharmacology, University of Colorado Anschutz Medical Campus and Center for Biological Physics and Department of Physics, Arizona State University, USA

[‡]Co-first authors

[*]Corresponding author: Diego Restrepo, diego.restrepo@cuanschutz.edu

Abstract

Background: Understanding viral infection of the olfactory epithelium is essential because smell loss can occur with coronavirus disease 2019 (COVID-19), caused by severe acute respiratory syndrome coronavirus clade 2 (SARS-CoV-2), and because the olfactory nerve is an important route of entry for viruses to the central nervous system. Specialized chemosensory epithelial cells that express the transient receptor potential cation channel subfamily M member 5 (TRPM5) are found throughout the airways and intestinal epithelium and are involved in responses to viral infection.

Results: Herein we performed deep transcriptional profiling of olfactory epithelial cells sorted by flow cytometry based on the expression of fluorescent protein markers for olfactory sensory neurons and TRPM5 in the mouse (*Mus musculus*). We find profuse expression of transcripts involved in inflammation, immunity and viral infection in TRPM5-expressing microvillous cells and olfactory sensory neurons. These cells express the *Tmprss2* transcript that encodes for a serine protease that primes the SARS-CoV-2 spike protein before entry into host cells. Intranasal infection with herpes simplex virus type 1 (HSV-1) elicited a decrease in olfactory sensory neurons.

Conclusion: Our study provides new insights into a potential role for TRPM5-expressing cells in viral infection of the olfactory epithelium. We find that, as found for solitary chemosensory cells (SCCs) and brush cells in the airway epithelium, and for tuft cells in the intestine, the transcriptome of TRPM5-expressing microvillous cells and olfactory sensory neurons indicates that they are likely involved in the inflammatory response elicited by viral infection of the olfactory epithelium.

47 **Keywords:** Olfactory sensory neurons, Microvillous cells, Viral infection, Immunity,

48 Inflammation, Mouse

Background

Self-reported loss of smell in a large fraction of patients with coronavirus disease 2019 (COVID-19), caused by severe acute respiratory syndrome coronavirus clade 2 (SARS-CoV-2), (Giacomelli et al., 2020; Parma et al., 2020; Yan et al., 2020a; Yan et al., 2020b) raises the question of how SARS-CoV-2 affects olfaction in a subset of patients. Entry of SARS-CoV-2 into cells is mediated by spike protein attachment to the SARS-CoV receptor ACE2 followed by spike protein priming by the serine protease TMPRSS2 (Hoffmann et al., 2020). Chemosensory cells found in the airway (SCCs/brush cells) and intestinal epithelium (tuft cells) express the transient receptor potential cation channel subfamily M member 5 (TRPM5) and other elements of the taste transduction pathway and have been implicated in immune and inflammatory responses to bacterial, viral and parasitic infection (Luo et al., 2019; Maina et al., 2018; O'Leary et al., 2019; Perniss et al., 2020; Rane et al., 2019; Saunders et al., 2014; Tizzano et al., 2010). In the olfactory epithelium TRPM5 and other proteins involved in taste transduction are also expressed in SCC-like microvillous cells (MVCs)(Genovese and Tizzano, 2018; Lin et al., 2008), which have been proposed to be involved in a protective response to high concentrations of odorants (Fu et al., 2018; Lemons et al., 2017). The ACE2 receptor and TMPRSS2 are expressed in support cells, stem cells, and MVCs (Brann et al., 2020; Fodoulian et al., 2020). However, whether MVCs play a role in viral infection or viral infection defense of the olfactory epithelium is unknown.

Herein, we performed transcriptional profiling of MVCs and a subset of olfactory sensory neurons (OSNs) expressing eGFP under control of the TRPM5 promoter (OSN_eGFP+ cells)(Lin et al., 2007; Lopez et al., 2014). In order to profile these low abundance cells we used

a modified version of Probe-Seq, which allows deep transcriptional profiling of specific cell types identified by fluorescent markers as the defining feature (Amamoto et al., 2019). We crossed a mouse expressing mCherry in the nuclei of OSNs under control of the OMP promoter (OMP-H2B::mCherry mice) with TRPM5-eGFP transgenic mice (Clapp et al., 2006) (OMP-H2B::mCherry/TRPM5-eGFP mice). We isolated cells from the olfactory epithelium and used fluorescence-activated cell sorting (FACS) to sort MVC_eGFP cells (mCherry negative and eGFP positive) and cells labeled by OMP-driven mCherry that did or did not express eGFP (OSN_eGFP+ and OSN_eGFP- cells) followed by transcriptional profiling by RNA sequencing (RNAseq).

Results

Fluorescence-activated cell sorting of cells isolated from the main olfactory epithelium. The olfactory epithelium of OMP-H2B::mCherry/TRPM5-eGFP mice expressed nuclear mCherry driven by the OMP promoter in the intermediate layer of the olfactory epithelium (Figures 1a), as expected for the location of nuclei of mature OSNs (Farbman and Margolis, 1980). eGFP expression driven by the TRPM5 promoter was found in MVCs, with cell bodies located mostly in the apical layer of the epithelium (asterisks), and at lower expression levels in a subset of OSNs double-labeled with mCherry (Figure 1a), consistent with earlier publications (Lin et al., 2008; Lin et al., 2007; Pyrski et al., 2017).

We proceeded to isolate cells from the main olfactory epithelium of OMP-H2B::mCherry/TRPM5-eGFP mice (see Methods, Figure 1b). Figure 1c shows two isolated OSNs with differential expression of eGFP. Using flow cytometry we found that fluorescence intensity of individual cells for mCherry and eGFP spanned several orders of magnitude (Figure 1d). We proceeded to sort three groups of cells: high mCherry-expressing cells with low and high eGFP fluorescence (presumably mature OSNs, these cells are termed OSN_eGFP- and OSN_eGFP+ cells respectively) and cells with low mCherry and high eGFP expression (MVC_eGFP, presumably MVCs). Reverse transcription quantitative PCR (RT-qPCR) showed that, as expected the OSN_eGFP- and OSN_eGFP+ cells have higher levels of OMP transcript than MVC_eGFP cells (Figure 1e,i), and OSN_eGFP+ cells and MVC_eGFP cells have higher levels of eGFP transcript compared to OSN_eGFP- cells (Figure 1e,ii). Furthermore, compared to OSN_eGFP- cells both the MVC_eGFP cells and OSN_eGFP+ cells expressed higher levels

of TRPM5 transcript (Figure 1e,iii) and choline acetyl transferase (ChAT)(Figure 1e,iv), a protein involved in acetylcholine neurotransmission that is expressed in MVCs (Ogura et al., 2011). The asterisks in Figure 1e denote significant differences tested with either t-test or ranksum with p-values below the p-value of significance corrected for multiple comparisons using the false discovery rate (pFDR)(Curran-Everett, 2000) (pFDR is 0.033 for OMP, 0.05 for TRPM5, 0.05 for EGFP and 0.03 for ChAT, n=8 for OMP OSN_eGFP-, 4 for OMP OSN_eGFP+ and 4 for MVC_eGFP cells).

The number of OSN_eGFP+ cells sorted by FACS is decreased when OMP-H2B::mCherry/TRPM5-eGFP mice are placed in ventilated cages. In our vivarium we have ventilated cages (HV cages) where air is mechanically exchanged with fresh air once every minute and static cages (LV cages) where air is exchanged passively through a filter in the cover. When we moved the OMP-H2B::mCherry/TRPM5-eGFP to HV cages we noticed a decrease in the number of OSN_eGFP+ cells sorted per mouse (Figures 2a,b and c), suggesting that changes in ventilation conditions affect TRPM5 promoter-driven expression of eGFP. Following this observation, mice were moved back to LV cages. We proceeded to study the dependence of the number of OSN_eGFP+ cells sorted on the number of days in LV vs. HV cages. The number of OSN_eGFP+ cells is positively correlated with the number of days the animal spends in LV cages (Figure 2d) and negatively correlated to the number of days the animals spend in the HV cages (Figure 2e). Generalized linear model (GLM) analysis found significant differences for the number of OSN_eGFP+ cells sorted as a function of the number of days in LV cages ($p<0.05$, 26 observations, 24 d.f., F-statistic = 5.64, p-value for GLM <0.05) and the number of days in HV cages ($p<0.05$, 26 observations, 24 d.f., F-statistic = 5.99, p-value for GLM <0.05). For RNAseq

129 experiments one FACS sort was done using cells from mice born and maintained in HV housing,
130 and the OSN_eGFP+ yield was low. Subsequently, we performed all FACS with cells isolated
131 from the olfactory epithelium of mice raised in LV cages.
132
133 **Coverage of TRPM5 transcript by RNAseq encompasses the full transcript in MVC_eGFP**
134 **cells and OSN_eGFP+ cells.** Pyrski and co-workers did not find full-length TRPM5 transcript
135 in reverse transcriptase polymerase chain reactions with mRNA extracted from isolated OSNs
136 from the adult mouse and did not find *in situ* signal in the OSN layer of the olfactory epithelium
137 for the full-length TRPM5 transcript (Pyrski et al., 2017). These investigators found full-length
138 TRPM5 transcript and strong *in situ* signal in MVCs. We find strong *in situ* signal for TRPM5 in
139 MVC_eGFP cells located in the apical layer of the olfactory epithelium (Figure 3aii, asterisks).
140 In addition, we find sparse TRPM5 *in situ* labeling in the nuclear OSN layer (Figure 3aii,
141 arrows). In order to gain a better understanding of which TRPM5 transcript is expressed in OSNs
142 we performed an analysis of TRPM5 transcript coverage for the RNAseq performed with RNA
143 from the different groups of cells sorted by FACS. Consistent with *in situ* labeling, TRPM5
144 transcript was significantly higher in OSN_eGFP+ cells compared to OSN_eGFP- cells and in
145 MVC_eGFP cells compared to OSN_eGFP- cells in both male and female adult mice (Figures
146 3b,c). To explore RNA sequencing coverage of individual *Trpm5* exons, we computed read
147 depth over the sequence of the *Trpm5* gene for each sample. We found coverage for all exons in
148 OSN_eGFP+ cells and for all exons except exon 1 and 5'UTR1 in MVC_eGFP cells, but there
149 was no coverage in OSN_eGFP- cells (Figures 3b,c). GLM analysis found statistically
150 significant differences for exons ($p<0.001$, 450 observations, 446 d.f., F-statistic = 33.8, p-value
151 for GLM <0.001), but no overall significance between MVC and OSN_eGFP+ groups ($p>0.05$,

450 observations, 446 d.f., F-statistic = 33.8, p-value for GLM <0.001). However, post-hoc ranksum tests did yield significant differences between MVC and OSN_eGFP+ groups for exon 1 and 5'UTR1 (p<pFDR=0.0033). We observed no differences in coverage between male and female mice (within MVC_eGFP cells: p>0.05, 210 observations, 206 d.f., F-statistic = 22.8, p value for GLM <0.001; within OSN_GFP+: p>0.05, 240 observations, 236 d.f., F-statistic = 11.5, p value for GLM <0.001). Together, these data suggest that both OSN_eGFP+ cells and MVC_eGFP cells are capable of expressing full-length TRPM5 transcript.

RNAseq indicates that OSN_eGFP+, OSN_eGFP- and MVC are three distinct groups of chemosensory cells in the mouse olfactory epithelium. Differential gene expression analysis of the RNAseq data was used to compare the three olfactory epithelium cell groups sorted by FACS. We found that expression of 2000 genes was significantly higher in OSN_eGFP+ compared to OSN_eGFP-, and expression of 1821 genes was lower in OSN_eGFP+ cells (Figure 4 -figure supplement 1 shows the results of RNAseq and Figure 4 -figure supplement 2 shows the metadata). Figure 4a shows expression levels for the transcripts that showed the largest differences between OSN_eGFP+ and OSN_eGFP- cells. The transcripts for TRPM5 and eGFP were among the top 10 genes whose transcription was higher in OSN_eGFP+ compared to OSN_eGFP- with 105-fold and 42-fold increases respectively. This top 10 OSN_eGFP+ upregulated group also includes *Avil* and *Adgrg6* that are involved in remodeling processes after peripheral nerve injury (Chuang et al., 2018; Jablonka-Shariff et al., 2020) and *Espn*, encoding for espin, a protein playing a structural role in microvilli of chemosensory cells (Sekerkova et al., 2004). Interestingly, the olfactory activity-dependent protein S100a5 (Fischl et al., 2014) is found among the top 10 OSN_eGFP+ downregulated transcripts suggesting that in these mice

the OSN_eGFP+ are not stimulated by the odorants in their housing environment (Figure 4a). Additionally, a majority of the olfactory receptors show decreased transcription in OSN_eGFP+ compared to OSN_eGFP- cells (Figures 4a,b) and the volcano plot for olfactory receptor transcript expression shows only 25 olfactory receptors show increased expression in OSN_eGFP+ cells (Figure 4c, based on fold change > 4 and average expression > 100 counts, Table 1).

Expression of 4386 genes was significantly higher in MVC_eGFP cells compared to OSN_eGFP- cells, and expression of 5630 genes was lower in MVC_eGFP cells (Figure 5 – figure supplement 1). Transcripts for 550 olfactory receptors were lower in MVC_eGFP cells (Figure 5 – figure supplement 1), and no olfactory receptors were upregulated in MVC_eGFP cells compared to OSN_eGFP-. Figure 5a shows expression levels for the transcripts with the largest differences between MVC_eGFP cells and OSN_eGFP- cells. Six of the transcripts that are within the top 10 upregulated genes found in MVC_eGFP cells compared to OSN_eGFP- cells (Figure 5a) are also found within the 10 top upregulated transcripts when OSN_eGFP+ cells are compared to OSN_eGFP- cells (Figure 4a)(*Adgrg6*, *Avil*, *Cd24a*, *eGFP*, *Espn* and *Trpm5*). TRPM5 and eEGFP were among the top 10 genes whose transcription was higher in MVC_eGFP cells compared to OSN_eGFP- cells with 1471-fold and 75-fold differences respectively. Interestingly, *Pou2f3*, a transcription factor important in differentiation of MVCs (Yamaguchi et al., 2014; Yamashita et al., 2017), is found within the top 10 upregulated genes found in MVC_eGFP cells compared to OSN_eGFP- (Figure 5a) and is also significantly higher in OSN_eGFP+ cells compared to OSN_eGFP- cells (Figure 5 – figure supplement 1). Finally, *OMP* and *s100a5*, genes for two proteins expressed in mature OSNs (Farbman and Margolis,

198 1980; Fischl et al., 2014), were among the top 10 downregulated transcripts in MVC_eGFP cells
199 compared to OSN_eGFP- cells (Figure 5a).
200
201 We found expression of 3068 genes which was significantly higher in MVC_eGFP cells
202 compared to OSN_eGFP+ cells, and expression of 4060 genes was lower in MVC_eGFP cells
203 (Figure 5 – figure supplement 2). Figure 5b shows expression levels for the genes that showed
204 the largest differences between MVC and OSN_eGFP+ cells. Among the 10 genes that are
205 highly expressed in OSN_eGFP+ cells compared to MVC_eGFP cells we find *Pde4a,* a gene
206 expressed in mature OSNs (Juilfs et al., 1997) (*OMP* is also significantly higher in OSN_eGFP+
207 cells, but is not among the top 10 genes, Figure 5 – figure supplement 2). Interestingly, *Hcn2*, a
208 gene that encodes for a hyperpolarization-activated cAMP channel that has been postulated to
209 participate in OSN axon growth and glomerular innervation (Mobley et al., 2010), is found in the
210 top 10 upregulated OSN_eGFP+ genes. Finally, the gene encoding for the synaptic protein
211 Snap25 is found in the top 10 upregulated lists for both OSN_eGFP+ and OSN_eGFP- indicating
212 that both OSNs are involved in synaptic transmission (Figures 5a and b).
213
214 We did not find major differences in transcriptome profiling between males and females for
215 genes that were differentially expressed between the three cell groups (Figure 5 – figure
216 supplement 3,4). We found a substantial number of olfactory receptor genes that were
217 differentially expressed between males and females (Figure 5 – figure supplement 4).
218 Surprisingly, the differentially expressed olfactory receptors differed from receptors identified by
219 van der Linden et al. (van der Linden et al., 2018). Finally, we compared expression of
220 transcripts involved in taste transduction, canonical olfactory transduction, and non-canonical

OSNs (Figure 4d). The non-canonical OSNs considered here included guanilyl-cyclase D (GC-D) OSNs (Juilfs et al., 1997), Trpc2 OSNs (Omura and Mombaerts, 2014) and Cav2.1 OSNs (Pyrski et al., 2018). Both OSN_eGFP+ and OSN_eGFP- expressed low levels of *Cancna1a* encoding for Cav2.1 and *Trpc2*. OSN_eGFP- expressed higher levels of Trace amine-associated receptors (Liberles, 2015) than OSN_eGFP+ cells. Both OSN_eGFP+ and OSN_eGFP- expressed transcripts for OMP, BBS1 and 2 and proteins involved in the canonical olfactory transduction pathway, markers of canonical OSNs.

Gene ontology enrichment analysis reveals differences in chemosensory transduction and synaptic vesicle function between the three groups of cells. Perusal of the top differences between the three cell groups suggested that these are distinct chemosensory cell types found in the olfactory epithelium. Both OSN_eGFP+ and OSN_eGFP- share expression of OSN-specific transcripts, express distinct subsets of olfactory receptors and differ in expression of the activity-dependent transcript *S100a5*, and MVC_eGFP cells differ from both OSN groups in expression of transcripts for synaptic transmission and for markers of mature OSNs and microvillous cells. In order to perform a thorough analysis of the differences between these chemosensory cell groups we performed an analysis of gene ontology (GO) enrichment for lists of genes related to chemosensory perception. When compared with either OSN_eGFP+ or OSN_eGFP- we found that MVC_eGFP cells were enriched for transcripts for the gene ontology list of sensory perception of sweet/umami taste (GO:0050916 and GO:0050917) (Figure 5d, Figure 5 – figure supplements 3,4) involving taste detection/transduction proteins that have been reported to be expressed in MVCs (Genovese and Tizzano, 2018; Hegg et al., 2010): *Gnat3*, encoding for gustducin, the G protein mediating sweet and umami taste transduction (McLaughlin et al.,

1992), *Itpr3*, encoding for the inositol-1,4,5-triphosphate receptor type 3 and *Tas1r3*, encoding for a gustducin-coupled receptor involved in umami and sweet taste (Damak et al., 2003; Zhang et al., 2003). Interestingly, the GO lists for sensory perception of sweet/umami taste (GO:0050916 and GO:0050917) and other lists for sensory and taste perception (GO:0050906, GO:0050912) are enriched in OSN_eGFP+ cells compared to OSN_eGFP- cells (Figure 4e, Figure 4 – figure supplement 3, including *Gnat3, Itpr3, Tas1r3*). Furthermore, gene ontology analysis for OSN_eGFP+ cells compared to OSN_eGFP- cells finds decreased enrichment for sensory perception of smell (GO:0007608) and G protein-coupled receptor signaling pathways (GO:0007186) that include a large number of olfactory receptors and transcripts encoding for proteins involved in peripheral olfaction such as *Gfy*, *Omp*, *Pde1c* and *Pde4a* (GO:0007608) and *Dgkg*, *Gng13*, *Itgb1*, *Nsg1* (GO:0007186). Finally, enrichment of gene ontology lists for synaptic vesicle function were decreased for MVC_eGFP cells compared with either OSN_eGFP+ or OSN_eGFP- cells (Figure 5c,d). Results of this gene ontology analysis of chemosensation and synaptic vesicle function reinforces the finding that the three cell groups in this study are distinct chemosensory cell types of the olfactory epithelium. OSN_eGFP+ cells are related to MVC_eGFP cells because of expression of taste perception gene ontology, but differ from MVC_eGFP cells in expression of olfactory receptors and transcripts related to synaptic function as expected for an OSN.

Gene ontology analysis finds enrichment of lists of viral-related, inflammation and immune transcripts in MVC_eGFP cells and OSN_eGFP+ cells. SCCs, tuft and brush cells have been implicated in responses to bacterial and viral infection, immunity and inflammation (Luo et al., 2019; Maina et al., 2018; O'Leary et al., 2019; Perniss et al., 2020; Rane et al., 2019; Saunders et

al., 2014; Tizzano et al., 2010; Ualiyeva et al., 2020). The fact that MVCs are closely related to these cells (Fu et al., 2018; Genovese and Tizzano, 2018; Ogura et al., 2011) lead us to search for gene ontology enrichment related to bacterial and viral infection, immunity and inflammation for MVC_eGFP cells. We found robust enrichment of these gene ontologies in MVC_eGFP cells and OSN_eGFP+ cells (Figures 4e, 5c,d). Transcripts related to viral infection that were higher in MVC_eGFP cells and OSN_eGFP+ cells compared to OSN_eGFP- cells (Figure 6) including those involved in viral entry into host cells, viral transcription and regulation of viral transcription, negative regulation of viral genome replication and negative regulation of viral process (Figures 4e, 5c, Figure 6 – figure supplements 1-3). We also found gene ontology enrichment in MVC_eGFP cells and OSN_eGFP+ cells compared to OSN_eGFP- cells for defense response to bacterium (Figure 6 – figure supplements 1-3).

Importantly, we also find enrichment for transcript expression for immunity and inflammation (Figures 4e, 5c,d and Figure 6 – figure supplements 1-3). Genes related to inflammation and immunity that were higher in MVC_eGFP cells and OSN_eGFP+ cells compared to OSN_eGFP- cells are shown in Figure 6 – figure supplements 4-7. Among these transcripts *IL25* and its receptor *Il17rb* are enriched in both MVC_eGFP cells and OSN_eGFP+ cells. In SCCs, brush cells and tuft cell generation of IL25 leads to a type 2 inflammation and stimulates chemosensory cell expansion in a sequence of events that also involves cysteinyl leukotrienes (Bankova et al., 2018; Luo et al., 2019; von Moltke et al., 2016). The presence of both *Il25* and *Il17rb* suggests an autocrine effect. Furthermore, both cell types displayed increased expression of transcripts encoding for enzymes involved in eicosanoid biosynthesis such as *Alox5*, *Ptgs1*

289 and *Ptgs2* that are found in brush cells in the airways (Bankova et al., 2018) and tuft cells in the
290 intestine (McGinty et al., 2020) where they drive type 2 immune responses.
291
292 **Acute infection with herpes simplex virus-1 (HSV-1) elicits a decrease in the fraction of**
293 **OSNs.** HSV-1 infects the olfactory epithelium in mice (Shivkumar et al., 2013). We found that
294 acute (5 DPI) high titer (1x 10^6 PFU/naris; McKrae strain) intranasal infection with HSV-1
295 elicited a decrease in the fraction of OSN_eGFP- and OSN_eGFP+ cells (Figure 7). GLM
296 analysis yielded significant effects for the fraction of OSN_eGFP- compared to MVCs ($p<0.001$)
297 and for the interaction between the fraction of OSN_eGFP- compared to MVCs and HSV-1 and
298 treatment ($p<0.001$, 75 observations, 69 d.f., GLM F-statistic=111 and p-value < 0.001, n=14
299 mice for control, n=11 mice for HSV-1 inoculation). Post-hoc t-test p-value was significant for
300 OSN_eGFP- and OSN_eGFP+ cells ($p < pFDR = 0.047$), but not for MVCs.
301
302
303
304
305

Discussion

We performed transcriptional profiling of three chemosensory cells in the mouse olfactory epithelium: MVC_eGFP cells and two types of OSNs: OSN_eGFP+ and OSN_eGFP-. We found that while the transcriptome of each of these cell types is distinct they share common features across groups. The two groups of OSNs share transcript expression for proteins expressed in OSNs such as OMP, olfactory transduction proteins, and proteins involved in synaptic function. Yet, they differ in olfactory receptor expression and OSN_eGFP+ express taste transduction transcripts and other transcripts found in SCCs such as *Il25* and *Pou2f3*. On the other hand, MVC_eGFP cells express transcripts encoding for taste transduction proteins and other transcripts found in SCCs such as *Pou2f3* but they do not express transcripts for proteins involved in olfactory transduction and synaptic function, and they do not express olfactory receptors. Finally, we found that MVC_eGFP cells and OSN_eGFP+ cells express a substantial number of transcripts involved in viral infection, inflammation and immunity.

Here we find that OSN_eGFP+ are OSNs expressing full-length TRPM5 in the adult mouse (Figure 3). This raises the question why our results differ from Pyrski and co-workers who did not find full-length TRPM5 in OSNs (Pyrski et al., 2017). Likely, this is due to differences in environmental conditions that alter the number of OSNs expressing TRPM5 in the adult mouse (Figure 2). Interestingly, consistent with our finding of TRPM5 expression in OSNs, analysis of scRNA data in the literature indicates that there are 8 OSNs expressing TRPM5 among 3209 OSNs in the data set from Ziegler and co-workers (Ziegler et al., 2020) and 3 OSNs expressing TRPM5 among 2113 OSNs in the data set from Wu and co-workers (Wu et al., 2018). Finally, OSN_eGFP+ express low levels of the activity-dependent transcript s100a5 (Fischl et al., 2014)

(Figure 4a) suggesting that these cells express olfactory receptors that are not stimulated by odorants present in the cage.

Gene ontology analysis revealed that MVC_eGFP cells (and OSN_eGFP+ cells to a lesser extent) are enriched in viral-related transcripts compared to OSN_eGFP- (Figures 4e, 5c,d, and Figure 6 – figure supplements 1-3). To infect cells, viruses must interact with host cell membranes to trigger membrane fusion and viral entry. Membrane proteins at the surface of the host cell are thus key elements promoting or preventing viral infection. Here we find that transcripts for several membrane proteins and cell adhesion molecules involved in viral entry are enriched in MVC_eGFP cells. *Plscr1* encodes a phospholipid scramblase which has been shown to promote herpes simplex virus (HSV) entry in human cervical or vaginal epithelial cells and keratinocytes (Cheshenko et al., 2018), and hepatitis C virus entry into hepatocytes (Gong et al., 2011). In contrast with its role in viral entry, PLSCR1 impairs the replication of other types of viruses in infected cells (influenza A virus (Luo et al., 2018), hepatitis B virus (Yang et al., 2012)). IFTM2 is another transmembrane protein that mediates viral entry. In contrast with PLSCR1, IFTM2 inhibits viral entry of human immunodeficiency virus (HIV, (Yu et al., 2015)), hepatitis C virus (Narayana et al., 2015), influenza A H1N1 virus, West Nile virus, and dengue virus (Brass et al., 2009). IFTM2 also inhibits viral replication (Brass et al., 2009) and protein synthesis (Lee et al., 2018). Nectins are transmembrane glycoproteins and constitute cell surface receptors for numerous viruses. There is wide evidence that HSV can enter host cells through Nectin-1 dependent mechanisms, particularly for neuronal entry (Kopp et al., 2009; Petermann et al., 2015; Sayers and Elliott, 2016; Shukla et al., 2012), and Nectin-4 appears essential for measles virus epithelial entry (Noyce and Richardson, 2012; Singh et al., 2015; Singh et al.,

2016). In addition to cell surface molecules, the mucus contains secreted proteins that confer protection against viruses to the underlying cells. Glycoproteins are major constituents of mucus and exhibit multiple pathogens binding-sites. We found the *Ltf* transcript in MVC_eGFP cells, which encodes for lactotransferrin. Lactotransferrin is a globular glycoprotein widely represented in the nasal mucus with anti-viral activity against Epstein-Barr virus (Zheng et al., 2014; Zheng et al., 2012), HSV (Shestakov et al., 2012; Valimaa et al., 2009)) and Hepatitis C virus (Allaire et al., 2015).

Viruses have developed numerous strategies to overcome barrier mechanisms to enter the cells. After viral entry infected cells have other resources to fight against viral infection by disrupting the production of new viral particles, limiting inflammation processes and activating innate immune responses. For example, TRIM25 is an ubiquitin ligase that activates retinoic acid-inducible gene I (RIG-I) to promote the antiviral interferon response (Gack et al., 2007). Furthermore, influenza A virus targets TRIM25 to evade recognition by the host cell (Gack et al., 2009). In addition, TRIM25 displays a nuclear role in restricting influenza A virus replication (Meyerson et al., 2017). Zc3h12a, also known as MCPIP-1, inhibits hepatitis B and C virus replication, reduces virus-induced inflammation (Li et al., 2020; Lin et al., 2014), and exerts antiviral effects against influenza A virus (Dong et al., 2017). Finally, *Pou2f3* also called *Skn1a*, encodes for a key regulator for the generation of TRPM5-expressing cells in various epithelial tissues (Yamashita et al., 2017). *Pou2f3* transcript was increased in MVC_eGFP cells (and to a lesser extent in OSN_eGFP+) compared to OSN_eGFP-. *Skn1a/Pou2f3*-deficient mice lack intestinal tuft cells and have defective mucosal type 2 responses to helminth infection in the intestine (Gerbe et al., 2016). Finally, both OSN_eGFP+ and MVC_eGFP cells express Il25, an

interleukin that is involved in the inflammatory response of TRPM5-expressing epithelial cells in the airway epithelium and the gut (O'Leary et al., 2019), and in the skin Il25 expression leads to disruption of the epithelium and enhances HSV-1 and vaccinia virus replication (Kim et al., 2013).

Our findings of expression of virally relevant transcripts in MVC_eGFP cells complement published studies on the role of MVC-related SCCs in viral infection. In the trachea, viral-associated formyl peptides activate SCCs to release acetylcholine and activate mucocilliary clearance by ciliated cells (Perniss et al., 2020). This activation is mediated by the TRPM5 transduction pathway in the SCC and muscarinic acetylcholine receptors in the ciliated cell. In a similar manner in the olfactory epithelium MVCs respond to ATP, which is involved in activating mucociliary movement by releasing acetylcholine and activating adjacent sustentacular cells through a muscarinic receptor (Fu et al., 2018). Therefore, viral infection could result in activation of MVCs resulting in activation of mucociliary clearance by adjacent sustentacular cells. In addition, in the anterior olfactory epithelium, where there is a higher density of MVCs, mice exposed to mild odorous irritants exhibited a time-dependent increase in apoptosis and a loss of mature OSNs without a significant increase in proliferation or neurogenesis (Lemons et al., 2020). This MVC-induced apoptosis could contribute to the decrease in the fraction of OSNs elicited by intranasal inoculation of HSV-1 (Figure 7). Future experiments are necessary to determine whether activation of MVCs by viruses could lead to loss of mature OSNs contributing to smell loss after viral infection. We did not find changes in MVC cell number after acute infection with HSV-1 (Figure 7c,iii). Interestingly, in the mouse distal lung, where there is no expression of SCCs, there was de novo generation of SCCs after infection

399 with A/H1N1/PR/8 influenza virus (Rane et al., 2019) raising the question whether longer virus
400 exposure could alter MVC number in the olfactory epithelium. Finally, because we find high
401 expression of transcripts involved in Type 2 immune response in MVCs viral activation of these
402 cells could result in activation of cytokine-induced inflammation by long-term horizontal basal
403 cells that activate type 1 immune responses within the olfactory epithelium (Chen et al., 2019).
404
405 The olfactory epithelium provides direct viral access to the brain through the olfactory nerve.
406 Whether this olfactory path constitutes route of entry for viruses to the brain is a matter of
407 intense discussion, especially because some viruses are postulated to be involved in
408 encephalopathy and neurodegenerative disorders (Dando et al., 2014; Doty, 2008). Our findings
409 that these TRPM5-bearing OSN_eGFP+ cells are enriched in virally-related genes suggests that
410 these cells may be involved in or prevention of viral entry into the brain (and these two
411 alternatives are not exclusive since they may be different for different viruses). On the one hand,
412 we identified transcripts encoding for viral receptors in OSN_eGFP+ cells, suggesting that
413 viruses can enter these OSNs. If viral particles were to enter the OSNs they could reach the
414 olfactory bulb through anterograde transport along the olfactory nerve and from the olfactory
415 bulb, viruses can spread throughout the brain along the olfactory bulb-hippocampus route. On
416 the other hand, we found enrichment for transcripts encoding for proteins involved in limiting
417 viral infection and promoting immune and anti-inflammatory responses in OSNs_eGFP+ and
418 MVC_eGFP cells. In this case, viral spread to the brain would be prevented. Finally, the
419 olfactory epithelium is innervated by the trigeminal nerve, and substance P immunostaining is
420 closely associated with subsets of MVCs (Lin et al., 2008). This raises the question whether an
421 interaction between MVCs and trigeminal nerve fibers could participate in local inflammation as

found for SCCs (Saunders et al., 2014), and could modulate the entry of virus to the brain stem through the trigeminal nerve. Future experiments are necessary to study the potential role of MVC_eGFP cells and OSNs_eGFP+ in viral infection of the olfactory epithelium and the brain.

Recently, due to the current COVID-19 pandemic, researchers have focused their attention on investigating SARS-CoV-2 mechanism of entry into cells. SARS-CoV-2 targets mainly cells of the respiratory pathway where viral entry is mediated by ACE2 and TMPRSS2 (Hoffmann et al., 2020). Because numerous patients reported loss of smell (Giacomelli et al., 2020; Parma et al., 2020; Yan et al., 2020a; Yan et al., 2020b), researchers wondered about the mechanism for SARS-CoV-2 infection of the olfactory epithelium. In our study, we found the *Tmprss2* transcript was significantly increased in MVC_eGFP cells and OSN_eGFP+ compared to OSN_eGFP- (Figure 6). We did not find *Ace2* enrichment in these cells, but this may be due to inefficiency in finding with RNAseq low abundance transcripts like *Ace2* (Ziegler et al., 2020). Transcriptional profiling of single cells in the olfactory epithelium from other laboratories found expression of transcripts for both *Tmprss2* and *Ace2* in in sustentacular cells and stem cells, and at lower levels in MVCs (Brann et al., 2020; Fodoulian et al., 2020). Viral infection of sustentacular cells may explain loss of smell because these cells play a key role in supporting olfactory function by providing glucose for the energy necessary for olfactory transduction in the OSN cilia (Villar et al., 2017). Importantly, type I interferons, and to a lesser extent type II interferons induced by response of the host to SARS-CoV-2, and infection by other viruses inducing the interferon pathway increases *Ace2* expression in the nasal epithelium (Ziegler et al., 2020). MVCs may play a role in SARS-CoV-2 infection of the olfactory epithelium because these cells may participate in activating inflammation of the epithelium that elicits type 1

immune response (Chen et al., 2019). Finally, our finding of transcripts involved in viral entry, replication and defense in a subset of OSNs raises the question whether viruses enter the central nervous system through the olfactory nerve (Bilinska et al., 2020). This is relevant to the potential long term effect of SARS-CoV-2 and other viruses in neurological and neurodegenerative disorders (De Felice et al., 2020). Our study provides new insights into a potential role for TRPM5-expressing cells in viral infection of the main olfactory epithelium.

Conclusion

Here we compared the transcriptome of OSNs that do not express TRPM5 (OSN_eGFP-) to a small fraction of cells that express TRPM5 (MVC_eGFP cells and OSN_eGFP+ cells) in the olfactory epithelium. We find that transcript expression in these three types of cells is distinct. OSN_eGFP- and OSN_eGFP+ cells share transcripts expressed in OSNs, while OSN_eGFP+ and MVCs share expression of transcripts found in SCCs and brush cells in the airways and tuft cells of the intestine. Interestingly, OSN_eGFP+ and MVCs express transcriptomes within the gene ontology transcript groups for immunology, inflammation and viral infection.

Abbreviations

COVID-19: Coronavirus disease 2019

DPI: Days post infection

eGFP: Enhanced green fluorescent protein

FACS: Fluorescence-activated cell sorting

FDR: False discovery rate

GLM: Generalized linear model

GO: Gene ontology

MVCs: Microvillous cells

OMP: Olfactory marker protein

OSNs: Olfactory sensory neurons

PSF: Point spread function

SARS-CoV-2: Severe acute respiratory syndrome coronavirus clade 2

SSC: Saline-sodium citrate

SSCT: SSC with tween

TRPM5: Transient receptor potential cation channel subfamily M member 5

Methods

Key Resources Table

REAGENT TYPE	REAGENT or RESOURCE	SOURCE	IDENTIFIER	ADDITIONAL INFORMATION
Chemical compound, drug	BrainPhys Neuronal Medium	Stemcell Technologies		Product # 05791
Chemical compound, drug	Dispase II	Sigma		Product # D4693
Chemical compound, drug	AcGFP1/eGFP calibration beads	Takara		Flow cytometry calibration beads Product # 632594
Chemical compound, drug	mCherry calibration beads	Takara		Flow cytometry calibration beads Product # 632595
Chemical compound, drug	RQ1 RNase-free DNase	Promega		Product # M6101
Chemical compound, drug	Papain	Sigma		Product # P3125
Chemical compound, drug	Paraformaldehyde (32%)	Electron Microscopy Sciences		Product # 157145
Chemical compound, drug	RNAprotect Tissue Reagent	Qiagen		Product # 76526
Chemical compound, drug	RNeasy Plus Micro Kit	Qiagen		Product # 74034
Chemical compound, drug	High Capacity c-DNA Reverse Transcription kit	ABI		
Chemical compound, drug	18s rRNA	PE ABI		
Strain, strain background	TRPM5-eGFP	Dr. Robert Margolskee (Clapp et al., 2006)		
Strain, strain background	OMP-H2B::Cherry	Generated for this publication		This mouse will be deposited in Jackson Laboratories
Software, algorithm	MATLAB_R2018a	Mathworks	RRID: SCR_001622	
Software, algorithm	Illustrator	Adobe	RRID: SCR_010279	
Software, algorithm	Photoshop	Adobe	RRID: SCR_014199	

Software, algorithm	InDesign	Adobe		
Software, algorithm	MoFlo Astrios Summit Software (6.3.1.16945).	Beckman Coulter		
Software, algorithm	BBMap (BBDuk)		RRID:SCR_016968	
Software, algorithm	Salmon v1.2.1	https://combine-lab.github.io/salmon/	RRID:SCR_017036	(Patro et al., 2017)
Software, algorithm	DeSEQ2 v1.28.0	bioconductor.org https://bioconductor.org/packages/release/bioc/html/DESeq2.html	RRID:SCR_015687	(Love et al., 2014)
Software, algorithm	TopGO, v2.40.0		RRID:SCR_014798	
Software, algorithm	pHeatmap, 1.0.12		RRID:SCR_016418	
Software, algorithm	Ensembl GRCm38, v99			
Software, algorithm	R, v4.0		RRID:SCR_001905	
Software, algorithm	Tximport, v1.16.0		RRID:SCR_016752	
Software, algorithm	SAMtools	SAMtools http://samtools.sourceforge.net/	RRID:SCR_002105	(Li et al., 2009)
Software, algorithm	Bedtools		RRID:SCR_006646	
Software, algorithm	STAR v2.5.3a	https://github.com/alexdobin/STAR	RRID:SCR_015899	
Software, algorithm	Sigmaplot, v12.5	Systat Software	RRID:SCR_003210	
Software, algorithm	Custom code for bioinformatics analysis	https://github.com/eric-d-larson/OE_TRPM5		

479

480 **Overview of the method for transcriptional profiling of low abundance cell populations.** For
481 transcriptional profiling of TRPM5-bearing MVC_eGFP cells and OSN_eGFP+ cells that
482 constitute a small fraction of the cells in the epithelium, we used FACS to separate the cell
483 populations targeted for RNAseq (Amamoto et al., 2019). In our experiments, we isolated the
484 cells from mice that expressed fluorescent marker proteins appropriate for cell sorting. OSNs
485 were expressing mCherry under the control of OMP promoter. eGFP was expressed in MVCs
486 and a subset of OSNs (OSN_eGFP+ cells) under control of the TRPM5 promoter.
487
488 **Generation of OMP-H2B::Cherry mice**. A PacI cassette containing PacI-H2B::mCherry-pA
489 PGK-puro-pA-PacI was inserted into an OMP gene-targeting vector (pPM9)(Mombaerts et
490 al., 1996), which replaces the OMP coding sequence with the PacI cassette and expresses a
491 H2B::mCherry fusion protein. Animals are maintained in a mixed 129/B6 background.
492
493 **Animals.** Mice with TRPM5-driven eGFP expression (Clapp et al.,2006) were crossed with
494 OMP-H2B::Cherry mice. The TRPM5-eGFP mice were obtained with written informed consent
495 from Dr. Robert Margolskee. Both lines were maintained separately as homozygous and
496 backcrossed regularly. Experiments were performed on mice from the F1 generation cross of
497 TRPM5-eGFP and OMP-H2B::Cherry mice (OMP-H2B::mCherry/TRPM5-eGFP). PCR was
498 used to verify genotype of experimental mice for eGFP and mCherry expression. Both male and
499 female mice were used for experiments with ages ranging from 3- 8 months. Estrous and cage
500 mate information was collected for all female mice in conjunction with experimental use. Mice
501 were housed in passive air exchange caging under a 12:12 light/dark cycle and were given food
502 and water *ad libitum*. Mice were housed in the National Institutes of Health approved Center for

Comparative Medicine at the University of Colorado Anschutz Medical Campus. All procedures were performed in compliance with University of Colorado Anschutz Medical Campus Institutional Animal Care and Use Committee (IACUC) that reviews the ethics of animal use.

Tissue dissociation of the olfactory epithelium. Following euthanasia via CO2 inhalation, the olfactory epithelium was immediately removed from the nasal cavity and epithelial tissue was separated from the bone in the turbinates. Care was taken not to include respiratory epithelium. The epithelium was dissociated enzymatically with Dispase II (2 mg/ml) diluted in Ringer's solution (145mM NaCl, 5mM KCL, 20mM HEPES, 1mM $MgCL_2$, 1mM $CaCl_2$, 1mM Ny-Pyruvate, 5mM Glucose) (~25 minutes at 37^0C) followed by an incubation in a papain plus Ca/Mg++ free Ringer's solution (Ca/Mg++ free Ringer's: 145mM NaCl, 5mM KCL, 20mM HEPES, 1mM Ny-Pyruvate, 1mM EDTA , L-cysteine: 1mg L-cysteine /1.5mL Ca/Mg++ free Ringer's, Papain:1-3ul/1mL Ca/Mg++ free Ringer's), for ~40-45 minutes at 37^0C. Following incubation, DNase I (Promega) at 0.05U/µl and RNAse free 10x Reaction buffer (1:20) were added to solution and the tissue was gently triturated using a ~1mm opening pipette. Isolated OSNs were collected from supernatants via centrifugation and resuspended in cell sorting medium of 1x PBS (diluted from commercial 10x PBS, pH 7.4) and BrainPhys Neuronal Medium (Stemcell Technologies). Initially, isolated cells were examined with a confocal microscope to confirm efficacy of dissociation methods, and examine cell types and fluorescence. For RNAseq, cells were strained through a 40 µm cell strainer and kept on ice until sorted via flow cytometry.

525 **Flow cytometry.** Fluorescence activated cell sorting was performed in the University of
526 Colorado Cancer Center Flow Cytometry Core on a Beckman Coulter MoFlo Astrios EQ using
527 MoFlo Astrios Summit Software (6.3.1.16945). eGFP signal was detected using a 488 nm laser
528 and a bandpass 526/52nm collection filter. mCherry signal was detected using a 561 nm laser
529 and a bandpass 614/20 nm collection filter. The 488nm laser was also used to detect light
530 scatter. The threshold was set at 3%. Gating was set to exclude doublets and optimized as cell
531 populations emerged based on fluorescent markers. Flow cytometry calibration beads for
532 AcGFP1/eGFP and mCherry (Takara, 632594, 632595) were used as fluorescence intensity
533 controls. Olfactory epithelium cell suspensions from wild type and OMP-H2B::Cherry mice or
534 TRPM5-eGFP mice were sorted as controls for auto fluorescence for eGFP and mCherry
535 populations respectively. Cells were sorted into RNAprotect Tissue Reagent (Qiagen).
536
537 **RNA-extraction.** Total RNA was extracted from sorted, pooled cells from each cell population
538 using the RNeasy Plus Micro Kit (Qiagen) according to the manufacturers recommended
539 protocol.
540
541 **RT-qPCR.** Quantitative reverse transcription polymerase chain reaction (RT-qPCR) was used to
542 assess and confirm identities of cell types from each of the sorted cell populations. Following
543 total RNA extraction, RT-qPCR was performed in the PCR core at University of Colorado
544 Anschutz Medical Campus for the following markers: OMP, TRPM5, eGFP and ChAT. Primers
545 and probes used for eGFP, TRPM5 and OMP were described in (Oshimoto et al., 2013).
546 Predesigned primers and probes for ChAT were purchased from Life Technologies. The mRNA
547 for these targets was measured by RT-qPCR using ABI QuantStudio 7 flex Sequence detector.

548 1μg total RNA was used to synthesize cDNA using the High Capacity c-DNA Reverse
549 Transcription kit (ABI-P/N 4368814). cDNA was diluted 1: 2 before PCR amplification.
550
551 The TaqMan probes were 5'labeled with 6-carboxyfluorescein (FAM). Real time PCR reactions
552 were carried out in MicroAmp optical tubes (PE ABI) in a 25 μl mix containing 8 % glycerol,
553 1X TaqMan buffer A (500 mM KCl, 100 mM Tris-HCl, 0.1 M EDTA, 600 nM passive
554 reference dye ROX, pH 8.3 at room temperature), 300 μM each of dATP, dGTP, dCTP and 600
555 μM dUTP, 5.5 mM MgCl2, 1X primer-probe mix, 1.25 U AmpliTaq Gold DNA and 5 μl
556 template cDNA. Thermal cycling conditions were as follows: Initiation was performed at 50°C
557 for 2 min followed by activation of TaqGold at 95°C for 10 min. Subsequently 40 cycles of
558 amplification were performed at 95°C for 15 secs and 60°C for 1 min. Experiments were
559 performed with duplicates for each data point. Each PCR run included the standard curve (10
560 fold serially diluted pooled cDNA from control and experimental samples), test samples, no-
561 template and NORT controls. The standard curve was then used to calculate the relative
562 amounts of targets in test samples. Quantities of targets in test samples were normalized to the
563 corresponding 18s rRNA (PE ABI, P/N 4308310).
564
565 **RNA sequencing and pre-processing.** RNA quality control, library preparation, and sequencing
566 were performed at the University of Colorado Genomics and Microarray core. Extracted RNA
567 was used as the input for the Nugen Universal Plus mRNA-seq kit (Redwood City, CA) to build
568 stranded sequencing libraries. Indexed libraries were sequenced using an Illumina
569 NovaSEQ6000. Library preparation and sequencing was performed in two batches, separated by
570 gender. 11 female samples were sequenced with an average depth of 37.3 million +/- SD of 6.5

million read pairs, and 25 male samples were sequenced with an average depth of 34.8 million +/- SD of 3.5 million read pairs. Metadata for the samples submitted are shown in Figure 4 – figure supplement 2. Raw BCL files were demultiplexed and converted to FASTQ format. Trimming, filtering, and adapter contamination removal was performed using BBDuk (Bushnell).

RNA Sequencing Analysis. Transcript abundance was quantified from trimmed and filtered FASTQ files using Salmon v1.2.1(Patro et al., 2017) and a customized Ensembl GRCm38 (release 99) transcriptome (Zerbino et al., 2018). A customized version of the transcriptome was prepared by appending FASTA sequences of eGFP and mCherry to the GRCm38 FASTA file. The corresponding gene transfer format (GTF) file was modified accordingly to incorporate the new transcripts. Transcript abundance was summarized at the gene level using the TxImport (Soneson et al., 2015) package in R. Differential gene expression was quantified using DESeq2 (Love et al., 2014) with default parameters after removing genes with an average count of < 5 reads in each group. Significance was determined by FDR-adjusted p-value < 0.05. TopGO was used for gene ontology analysis (Alexa and Rahnenfuhrer, 2020). The input to TopGO was a list of significant DEGs and a list of all detected genes in the dataset. Enrichment was calculated by dividing the number of detected genes by the number of expected genes within each ontology of the TopGO output. To make the bar graphs in Figures 4 and 5, enrichment scores of downregulated GO terms were multiplied by -1 for visualization. Heatmap visualization was performed using *pHeatmap* in R (Kolde, 2019).

TRPM5 exon coverage. To visualize exon coverage of *Trpm5*, trimmed and filtered FASTQ files were mapped to the Ensembl GRCm38 (version 99) using STAR (params, version 2.5.3a)(Dobin et al., 2013). The genome FASTA and GTF files were modified as described above. Read coverage was summarized by *Trpm5* exon using a combination of Samtools ('depth' and 'bedcov')(Li et al., 2009) and Bedtools (Quinlan and Hall, 2010). Data were compared using a Scheirer-Ray-Hare test in R (*rcompanion* package).

Tissue Preparation for Fluorescence Microscopy and *in situ*. For euthanasia, mice were anesthetized with ketamine/xylazine (20–100 _g/g of body weight), perfused transcardially with 0.1 M phosphate buffer (PBS) followed by a PBS-buffered fixative (EMS 32% Paraformaldehyde aqueous solution diluted to 4% with 1x PBS) . The nose was harvested and postfixed for 12 h before being transferred for cryoprotection into PBS with 20% sucrose overnight. The olfactory epithelium was cryosectioned coronally into 16 µm -thick sections mounted on Superfrost Plus slides (VWR, West Chester, PA).

In situ. *In situ* hybridization was performed with the hybridization chain reaction method (Choi et al., 2018) using HCR v3.0 Probe Sets, Amplifiers, and Buffers from Molecular Instruments, Inc. Frozen slides were allowed to thaw and dry, then immersed in 70% ethanol overnight at 4°C, and allowed to dry again completely. Slides were inverted and placed on a Plexiglas platform inside a humidified chamber; subsequent steps were performed using this setup. Slides were incubated in 10 µg/µl proteinase K for 10 minutes at 37°C, then pre-hybridized with HCR hybridization buffer (30% formamide buffer from Molecular Instruments) for 10 minutes at 37°C. *Trpm5-B3* probes and *OMP-B2* probes (0.4 pmol of each probe in 100 µl HCR

hybridization buffer per slide) were added, and slides were hybridized overnight at 37°C. Slides were briefly incubated in undiluted HCR Wash Buffer (30% formamide buffer from Molecular Instruments) at 37°C. Excess probes were removed by incubating slides for 15 minutes each at 37°C in solutions of 75% HCR Wash Buffer / 25% SSCT (5X SSC, 0.1% Tween, diluted in RNAse free water), 50% Buffer / 50% SSCT, 25% Buffer / 75% SSCT, and 100% SSCT. Slides were incubated in Amplification Buffer (Molecular Instruments) at room temperature for 30 minutes. B3 hairpins labeled with Alexa Fluor 647 and B2 hairpins labeled with Alexa Fluor 546 were prepared (6 pmol of each hairpin were heat shocked, then cooled for 30 minutes, and added to 100µl of Amplification Buffer) added to slides, and incubated overnight at room temperature. Excess hairpins were removed with three washes in SSCT at room temperature. Tissue was counterstained with DAPI, and slides were mounted using Invitrogen SlowFade Diamond Antifade Mountant (Thermo Fisher Scientific).

Fluorescence microscopy. Microscopy was performed with confocal microscopes (Nikon A1R or 3i Marianas). Images shown are flattened Z stacks. In situ images in Figure 3 were deconvolved in DeconvolutionLab 2 (Sage et al., 2017) using 10 rounds of Lucy-Richardson deconvolution (Lucy, 1974; Richardson, 1972) and a theoretical point spread function (PSF). The theoretical PSF was calculated using the Gibson-Lanni model (Gibson and Lanni, 1989) for 325 nm lateral and 800 nm axial pixel size, wavelength of the reporter dye molecule, and an air-immersion 20X NA 0.75 objective. Image was maximum projected and Gamma of 0.8 applied to the TRMP5 channel for viewing.

638 **Viral stocks.** HSV-1, McKrae strain (gift from Dr. David Bloom, University of Florida), was
639 used for all experiments. Viral stocks were prepared in Vero cells; infectious particles were
640 purified from the supernatant, aliquoted, and stored at -80C. Viral titers were determined via
641 plaque forming unit-(PFU) assays.
642
643 **Viral infection.** 3-6 month old OMP-H2B::mCherry/TRPM5-eGFP mice were lightly
644 anesthetized with isoflurane and inoculated intranasally with 10 µL of solution per naris (20 µL
645 total). The solution contained either HSV-1 (1x 10^6 PFU/naris; McKrae strain), or PBS (7.4 pH)
646 (sham control). Mice were randomly assigned to these groups. Mice were sacrificed at 5 days
647 post-infection (5 DPI). Controls included sham-treated mice (5), mice that were lightly
648 anesthetized (3), untreated mice housed in the BSL-2 facility (3) or the regular room (3). All
649 controls were used because ranksum tests corrected for multiple comparisons did not find
650 differences between these groups.
651
652 **Statistical analysis.** Statistical analysis was performed in Matlab (Mathworks, USA). Statistical
653 significance was estimated using a generalized linear model (GLM), with post-hoc tests for all
654 data pairs corrected for multiple comparisons using false discovery rate (Curran-Everett, 2000).
655 The post hoc comparisons between pairs of data were performed either with a t-test, or a ranksum
656 test, depending on the result of an Anderson-Darling test of normality. 95% CIs shown in the
657 figures as vertical black lines or shading bounding the lines were estimated by bootstrap analysis
658 of the mean by sampling with replacement 1000 times using the bootci function in MATLAB.
659
660
661

Declarations

Ethics approvals. Mouse experiments were carried out under guidelines of the National Institutes of Health in compliance with University of Colorado Anschutz Medical Campus Institutional Animal Care and Use Committee (IACUC).

Consent for publication. Not applicable.

Availability of data and materials. All data sequencing data are available in NCBI SRA https://www.ncbi.nlm.nih.gov/sra/PRJNA632936. The code used for bioinformatics analysis is found in https://github.com/eric-d-larson/OE_TRPM5

Competing interests. The authors declare no competing interests.

Funding. This work was supported by NIDCD DC014253 and NIA DC014253-04S1 (DR) and by the RNA Bioscience Initiative of the University of Colorado Anschutz Medical Campus (DS and DR). A Starr Stem Cell Grant (JA, AKH and PF) supported the production and characterization of the OMP-H2B::mCherry mouse strain. The funding bodies had no role in the experimental design or collection, analysis and interpretation of data or in writing the manuscript.

Authors' contributions. D.R., B.D.B., M.N. and V.R. conceptualized the project. B.D.B. performed FACS, qPCR and RNAseq experiments. E.D.L. performed genomic analysis. P.F.

685 generated the OMP-H2B::Cherry mice. D.S. designed and analyzed in situ experiments. M.N.,
686 A.N.B. and C.N. designed the HSV-1 inoculation experiments. C.N. and J.H.Jr. performed the
687 viral inoculation. M.L. performed literature search and wrote the section on viral infection in the
688 discussion. All authors contributed to writing and editing the manuscript.
689
690 ***Acknowledgements:*** We would like to acknowledge the support of Nicole Arevalo for laboratory
691 support, Jerome Artus and Anna-Katerina Hadjantonakis for the construction of the targeting
692 vector and production of OMP-H2B::Cherry mice.
693
694 ***Declaration of interests:*** The authors declare no competing interests.
695

References

Alexa, A., and Rahnenfuhrer, J. (2020). topGO: Enrichment Analysis for Gene Ontology (R Package).

Allaire, A., Picard-Jean, F., and Bisaillon, M. (2015). Immunofluorescence to Monitor the Cellular Uptake of Human Lactoferrin and its Associated Antiviral Activity Against the Hepatitis C Virus. J Vis Exp.

Amamoto, R., Garcia, M.D., West, E.R., Choi, J., Lapan, S.W., Lane, E.A., Perrimon, N., and Cepko, C.L. (2019). Probe-Seq enables transcriptional profiling of specific cell types from heterogeneous tissue by RNA-based isolation. Elife *8*.

Bankova, L.G., Dwyer, D.F., Yoshimoto, E., Ualiyeva, S., McGinty, J.W., Raff, H., von Moltke, J., Kanaoka, Y., Frank Austen, K., and Barrett, N.A. (2018). The cysteinyl leukotriene 3 receptor regulates expansion of IL-25-producing airway brush cells leading to type 2 inflammation. Sci Immunol *3*.

Bilinska, K., Jakubowska, P., Von Bartheld, C.S., and Butowt, R. (2020). Expression of the SARS-CoV-2 Entry Proteins, ACE2 and TMPRSS2, in Cells of the Olfactory Epithelium: Identification of Cell Types and Trends with Age. ACS Chemical Neuroscience.

Brann, D.H., Tsukahara, T., Weinreb, C., Lipovsek, M., Van den Berge, K., Gong, B., Chance, R., Macaulay, I.C., Chou, H.-j., Fletcher, R.*, et al.* (2020). Non-neuronal expression of SARS-

714 CoV-2 entry genes in the olfactory system suggests mechanisms underlying COVID-19-
715 associated anosmia. bioRxiv, 2020.2003.2025.009084.

716 Brass, A.L., Huang, I.C., Benita, Y., John, S.P., Krishnan, M.N., Feeley, E.M., Ryan, B.J.,
717 Weyer, J.L., van der Weyden, L., Fikrig, E.*, et al.* (2009). The IFITM proteins mediate cellular
718 resistance to influenza A H1N1 virus, West Nile virus, and dengue virus. Cell *139*, 1243-1254.

719 Bushnell, B. BBMap (SourceForge).

720 Chen, M., Reed, R.R., and Lane, A.P. (2019). Chronic Inflammation Directs an Olfactory Stem
721 Cell Functional Switch from Neuroregeneration to Immune Defense. Cell Stem Cell *25*, 501-513
722 e505.

723 Cheshenko, N., Pierce, C., and Herold, B.C. (2018). Herpes simplex viruses activate
724 phospholipid scramblase to redistribute phosphatidylserines and Akt to the outer leaflet of the
725 plasma membrane and promote viral entry. PLoS Pathog *14*, e1006766.

726 Choi, H.M., Schwarzkopf, M., Fornace, M.E., Acharya, A., Artavanis, G., Stegmaier, J., Cunha,
727 A., and Pierce, N.A. (2018). Third-generation in situ hybridization chain reaction: multiplexed,
728 quantitative, sensitive, versatile, robust. Development *145*, dev165753.

729 Chuang, Y.C., Lee, C.H., Sun, W.H., and Chen, C.C. (2018). Involvement of advillin in
730 somatosensory neuron subtype-specific axon regeneration and neuropathic pain. Proc Natl Acad
731 Sci U S A *115*, E8557-E8566.

732 Clapp, T.R., Medler, K.F., Damak, S., Margolskee, R.F., and Kinnamon, S.C. (2006). Mouse
733 taste cells with G protein-coupled taste receptors lack voltage-gated calcium channels and
734 SNAP-25. BMC Biol *4*, 7.

735 Curran-Everett, D. (2000). Multiple comparisons: philosophies and illustrations. AmJPhysiol
736 RegulIntegrComp Physiol *279*, R1-R8.

737 Damak, S., Rong, M., Yasumatsu, K., Kokrashvili, Z., Varadarajan, V., Zou, S., Jiang, P.,
738 Ninomiya, Y., and Margolskee, R.F. (2003). Detection of sweet and umami taste in the absence
739 of taste receptor T1r3. Science *301*, 850-853.

740 Dando, S.J., Mackay-Sim, A., Norton, R., Currie, B.J., St John, J.A., Ekberg, J.A.K., Batzloff,
741 M., Ulett, G.C., and Beacham, I.R. (2014). Pathogens Penetrating the Central Nervous System:
742 Infection Pathways and the Cellular and Molecular Mechanisms of Invasion. Clinical
743 Microbiology Reviews *27*, 691-726.

744 De Felice, F.G., Tovar-Moll, F., Moll, J., Munoz, D.P., and Ferreira, S.T. (2020). Severe Acute
745 Respiratory Syndrome Coronavirus 2 (SARS-CoV-2) and the Central Nervous System. Trends in
746 Neurosciences.

747 Dobin, A., Davis, C.A., Schlesinger, F., Drenkow, J., Zaleski, C., Jha, S., Batut, P., Chaisson,
748 M., and Gingeras, T.R. (2013). STAR: ultrafast universal RNA-seq aligner. Bioinformatics *29*,
749 15-21.

750 Dong, C., Sun, X., Guan, Z., Zhang, M., and Duan, M. (2017). Modulation of influenza A virus
751 replication by microRNA-9 through targeting MCPIP1. J Med Virol *89*, 41-48.

752 Doty, R.L. (2008). The olfactory vector hypothesis of neurodegenerative disease: is it viable?
753 Ann Neurol *63*, 7-15.

754 Farbman, A.I., and Margolis, F.L. (1980). Olfactory marker protein during ontogeny:
755 immunohistochemical localization. Developmental biology *74*, 205-215.

756 Fischl, A.M., Heron, P.M., Stromberg, A.J., and McClintock, T.S. (2014). Activity-dependent
757 genes in mouse olfactory sensory neurons. Chem Senses *39*, 439-449.

758 Fodoulian, L., Tuberosa, J., Rossier, D., Landis, B.N., Carleton, A., and Rodriguez, I. (2020).
759 SARS-CoV-2 receptor and entry genes are expressed by sustentacular cells in the human
760 olfactory neuroepithelium. bioRxiv, 2020.2003.2031.013268.

761 Fu, Z., Ogura, T., Luo, W., and Lin, W. (2018). ATP and Odor Mixture Activate TRPM5-
762 Expressing Microvillous Cells and Potentially Induce Acetylcholine Release to Enhance
763 Supporting Cell Endocytosis in Mouse Main Olfactory Epithelium. Front Cell Neurosci *12*, 71.

764 Gack, M.U., Albrecht, R.A., Urano, T., Inn, K.S., Huang, I.C., Carnero, E., Farzan, M., Inoue,
765 S., Jung, J.U., and Garcia-Sastre, A. (2009). Influenza A virus NS1 targets the ubiquitin ligase
766 TRIM25 to evade recognition by the host viral RNA sensor RIG-I. Cell Host Microbe *5*, 439-
767 449.

768 Gack, M.U., Shin, Y.C., Joo, C.H., Urano, T., Liang, C., Sun, L., Takeuchi, O., Akira, S., Chen,
769 Z., Inoue, S., *et al.* (2007). TRIM25 RING-finger E3 ubiquitin ligase is essential for RIG-I-
770 mediated antiviral activity. Nature *446*, 916-920.

771 Genovese, F., and Tizzano, M. (2018). Microvillous cells in the olfactory epithelium express
772 elements of the solitary chemosensory cell transduction signaling cascade. PLoS One *13*,
773 e0202754.

774 Gerbe, F., Sidot, E., Smyth, D.J., Ohmoto, M., Matsumoto, I., Dardalhon, V., Cesses, P.,
775 Garnier, L., Pouzolles, M., Brulin, B., *et al.* (2016). Intestinal epithelial tuft cells initiate type 2
776 mucosal immunity to helminth parasites. Nature *529*, 226-230.

777 Giacomelli, A., Pezzati, L., Conti, F., Bernacchia, D., Siano, M., Oreni, L., Rusconi, S.,
778 Gervasoni, C., Ridolfo, A.L., Rizzardini, G., *et al.* (2020). Self-reported olfactory and taste
779 disorders in SARS-CoV-2 patients: a cross-sectional study. Clin Infect Dis.

780 Gibson, S.F., and Lanni, F. (1989). Diffraction by a circular aperture as a model for three-
781 dimensional optical microscopy. J Opt Soc Am A *6*, 1357-1367.

782 Gong, Q., Cheng, M., Chen, H., Liu, X., Si, Y., Yang, Y., Yuan, Y., Jin, C., Yang, W., He, F., *et*
783 *al.* (2011). Phospholipid scramblase 1 mediates hepatitis C virus entry into host cells. FEBS Lett
784 *585*, 2647-2652.

785 Hegg, C.C., Jia, C., Chick, W.S., Restrepo, D., and Hansen, A. (2010). Microvillous cells
786 expressing IP3 receptor type 3 in the olfactory epithelium of mice. Eur J Neurosci *32*, 1632-
787 1645.

788 Hoffmann, M., Kleine-Weber, H., Schroeder, S., Kruger, N., Herrler, T., Erichsen, S.,
789 Schiergens, T.S., Herrler, G., Wu, N.H., Nitsche, A.*, et al.* (2020). SARS-CoV-2 Cell Entry
790 Depends on ACE2 and TMPRSS2 and Is Blocked by a Clinically Proven Protease Inhibitor. Cell
791 *181*, 271-280 e278.

792 Jablonka-Shariff, A., Lu, C.Y., Campbell, K., Monk, K.R., and Snyder-Warwick, A.K. (2020).
793 Gpr126/Adgrg6 contributes to the terminal Schwann cell response at the neuromuscular junction
794 following peripheral nerve injury. Glia *68*, 1182-1200.

795 Juilfs, D.M., Fulle, H.J., Zhao, A.Z., Houslay, M.D., Garbers, D.L., and Beavo, J.A. (1997). A
796 subset of olfactory neurons that selectively express cGMP-stimulated phosphodiesterase (PDE2)
797 and guanylyl cyclase-D define a unique olfactory signal transduction pathway. Proc Natl Acad
798 Sci U S A *94*, 3388-3395.

799 Kim, B.E., Bin, L., Ye, Y.M., Ramamoorthy, P., and Leung, D.Y.M. (2013). IL-25 enhances
800 HSV-1 replication by inhibiting filaggrin expression, and acts synergistically with Th2 cytokines
801 to enhance HSV-1 replication. J Invest Dermatol *133*, 2678-2685.

802 Kolde, R. (2019). pheatmap: Pretty Heatmaps (cran.r-project.org).

803 Kopp, S.J., Banisadr, G., Glajch, K., Maurer, U.E., Grunewald, K., Miller, R.J., Osten, P., and
804 Spear, P.G. (2009). Infection of neurons and encephalitis after intracranial inoculation of herpes
805 simplex virus requires the entry receptor nectin-1. Proc Natl Acad Sci U S A *106*, 17916-17920.

806 Lee, W.J., Fu, R.M., Liang, C., and Sloan, R.D. (2018). IFITM proteins inhibit HIV-1 protein
807 synthesis. Sci Rep *8*, 14551.

808 Lemons, K., Fu, Z., Aoude, I., Ogura, T., Sun, J., Chang, J., Mbonu, K., Matsumoto, I.,
809 Arakawa, H., and Lin, W. (2017). Lack of TRPM5-Expressing Microvillous Cells in Mouse
810 Main Olfactory Epithelium Leads to Impaired Odor-Evoked Responses and Olfactory-Guided
811 Behavior in a Challenging Chemical Environment. eNeuro *4*.

812 Lemons, K., Fu, Z., Ogura, T., and Lin, W. (2020). TRPM5-expressing Microvillous Cells
813 Regulate Region-specific Cell Proliferation and Apoptosis During Chemical Exposure.
814 Neuroscience *434*, 171-190.

815 Li, H., Handsaker, B., Wysoker, A., Fennell, T., Ruan, J., Homer, N., Marth, G., Abecasis, G.,
816 Durbin, R., and Genome Project Data Processing, S. (2009). The Sequence Alignment/Map
817 format and SAMtools. Bioinformatics *25*, 2078-2079.

818 Li, M., Yang, J., Zhao, Y., Song, Y., Yin, S., Guo, J., Zhang, H., Wang, K., Wei, L., Li, S.*, et al.*
819 (2020). MCPIP1 inhibits Hepatitis B virus replication by destabilizing viral RNA and negatively
820 regulates the virus-induced innate inflammatory responses. Antiviral Res *174*, 104705.

821 Liberles, S.D. (2015). Trace amine-associated receptors: ligands, neural circuits, and behaviors.
822 Current opinion in neurobiology *34*, 1-7.

823 Lin, R.J., Chu, J.S., Chien, H.L., Tseng, C.H., Ko, P.C., Mei, Y.Y., Tang, W.C., Kao, Y.T.,
824 Cheng, H.Y., Liang, Y.C., *et al.* (2014). MCPIP1 suppresses hepatitis C virus replication and
825 negatively regulates virus-induced proinflammatory cytokine responses. J Immunol *193*, 4159-
826 4168.

827 Lin, W., Ezekwe, E.A., Jr., Zhao, Z., Liman, E.R., and Restrepo, D. (2008). TRPM5-expressing
828 microvillous cells in the main olfactory epithelium. BMC Neurosci *9*, 114.

829 Lin, W., Margolskee, R., Donnert, G., Hell, S.W., and Restrepo, D. (2007). Olfactory neurons
830 expressing transient receptor potential channel M5 (TRPM5) are involved in sensing
831 semiochemicals. Proc Natl Acad Sci U S A *104*, 2471-2476.

832 Lopez, F., Delgado, R., Lopez, R., Bacigalupo, J., and Restrepo, D. (2014). Transduction for
833 Pheromones in the Main Olfactory Epithelium Is Mediated by the Ca2+-Activated Channel
834 TRPM5. J Neurosci *34*, 3268-3278.

835 Love, M.I., Huber, W., and Anders, S. (2014). Moderated estimation of fold change and
836 dispersion for RNA-seq data with DESeq2. Genome Biol *15*, 550.

837 Lucy, L.B. (1974). An iterative technique for the rectification of observed distributions. The
838 Astronomical Journal *79*, 745.

839 Luo, W., Zhang, J., Liang, L., Wang, G., Li, Q., Zhu, P., Zhou, Y., Li, J., Zhao, Y., Sun, N., *et al.*
840 (2018). Phospholipid scramblase 1 interacts with influenza A virus NP, impairing its nuclear
841 import and thereby suppressing virus replication. PLoS Pathog *14*, e1006851.

842 Luo, X.C., Chen, Z.H., Xue, J.B., Zhao, D.X., Lu, C., Li, Y.H., Li, S.M., Du, Y.W., Liu, Q.,
843 Wang, P., *et al.* (2019). Infection by the parasitic helminth Trichinella spiralis activates a Tas2r-
844 mediated signaling pathway in intestinal tuft cells. Proc Natl Acad Sci U S A *116*, 5564-5569.

845 Maina, I.W., Workman, A.D., and Cohen, N.A. (2018). The role of bitter and sweet taste
846 receptors in upper airway innate immunity: Recent advances and future directions. World J
847 Otorhinolaryngol Head Neck Surg *4*, 200-208.

848 McGinty, J.W., Ting, H.-A., Billipp, T.E., Nadjsombati, M.S., Khan, D.M., Barrett, N.A., Liang,
849 H.-E., Matsumoto, I., and von Moltke, J. (2020). Tuft-Cell-Derived Leukotrienes Drive Rapid
850 Anti-helminth Immunity in the Small Intestine but Are Dispensable for Anti-protist Immunity.
851 Immunity *52*, 528-541.e527.

852 McLaughlin, S.K., McKinnon, P.J., and Margolskee, R.F. (1992). Gustducin is a taste-cell-
853 specific G protein closely related to the transducins. Nature *357*, 563-569.

854 Meyerson, N.R., Zhou, L., Guo, Y.R., Zhao, C., Tao, Y.J., Krug, R.M., and Sawyer, S.L. (2017).
855 Nuclear TRIM25 Specifically Targets Influenza Virus Ribonucleoproteins to Block the Onset of
856 RNA Chain Elongation. Cell Host Microbe *22*, 627-638 e627.

857 Mobley, A.S., Miller, A.M., Araneda, R.C., Maurer, L.R., Muller, F., and Greer, C.A. (2010).
858 Hyperpolarization-activated cyclic nucleotide-gated channels in olfactory sensory neurons
859 regulate axon extension and glomerular formation. The Journal of neuroscience : the official
860 journal of the Society for Neuroscience *30*, 16498-16508.

861 Mombaerts, P., Wang, F., Dulac, C., Chao, S.K., Nemes, A., Mendelsohn, M., Edmondson, J.,
862 and Axel, R. (1996). Visualizing an olfactory sensory map. Cell *87*, 675-686.

863 Narayana, S.K., Helbig, K.J., McCartney, E.M., Eyre, N.S., Bull, R.A., Eltahla, A., Lloyd, A.R.,
864 and Beard, M.R. (2015). The Interferon-induced Transmembrane Proteins, IFITM1, IFITM2,
865 and IFITM3 Inhibit Hepatitis C Virus Entry. J Biol Chem *290*, 25946-25959.

866 Noyce, R.S., and Richardson, C.D. (2012). Nectin 4 is the epithelial cell receptor for measles
867 virus. Trends Microbiol *20*, 429-439.

868 O'Leary, C.E., Schneider, C., and Locksley, R.M. (2019). Tuft Cells-Systemically Dispersed
869 Sensory Epithelia Integrating Immune and Neural Circuitry. Annu Rev Immunol *37*, 47-72.

870 Ogura, T., Szebenyi, S.A., Krosnowski, K., Sathyanesan, A., Jackson, J., and Lin, W. (2011).
871 Cholinergic microvillous cells in the mouse main olfactory epithelium and effect of acetylcholine
872 on olfactory sensory neurons and supporting cells. J Neurophysiol *106*, 1274-1287.

873 Omura, M., and Mombaerts, P. (2014). Trpc2-Expressing Sensory Neurons in the Main
874 Olfactory Epithelium of the Mouse. Cell Reports *8*, 583-595.

875 Oshimoto, A., Wakabayashi, Y., Garske, A., Lopez, R., Rolen, S., Flowers, M., Arevalo, N., and
876 Restrepo, D. (2013). Potential role of transient receptor potential channel M5 in sensing putative
877 pheromones in mouse olfactory sensory neurons. PLoS One *8*, e61990.

878 Parma, V., Ohla, K., Veldhuizen, M.G., Nim, M.Y., Kelly, C.E., Reed, D.R., Hummel, T.,
879 Munger, S., and Hayes, J.E. (2020). More than just smell - COVID-19 is associated with severe
880 impairment of smell, taste, and chemesthesis. medRxiv, 2020.2005.2004.20090902.

881 Patro, R., Duggal, G., Love, M.I., Irizarry, R.A., and Kingsford, C. (2017). Salmon provides fast
882 and bias-aware quantification of transcript expression. Nature methods *14*, 417-419.

883 Perniss, A., Liu, S., Boonen, B., Keshavarz, M., Ruppert, A.L., Timm, T., Pfeil, U., Soultanova,
884 A., Kusumakshi, S., Delventhal, L.*, et al.* (2020). Chemosensory Cell-Derived Acetylcholine
885 Drives Tracheal Mucociliary Clearance in Response to Virulence-Associated Formyl Peptides.
886 Immunity *52*, 683-699 e611.

887 Petermann, P., Rahn, E., Thier, K., Hsu, M.J., Rixon, F.J., Kopp, S.J., and Knebel-Morsdorf, D.
888 (2015). Role of Nectin-1 and Herpesvirus Entry Mediator as Cellular Receptors for Herpes
889 Simplex Virus 1 on Primary Murine Dermal Fibroblasts. J Virol *89*, 9407-9416.

890 Pyrski, M., Eckstein, E., Schmid, A., Bufe, B., Weiss, J., Chubanov, V., Boehm, U., and Zufall,
891 F. (2017). Trpm5 expression in the olfactory epithelium. Mol Cell Neurosci *80*, 75-88.

892 Pyrski, M., Tusty, M., Eckstein, E., Oboti, L., Rodriguez-Gil, D.J., Greer, C.A., and Zufall, F.
893 (2018). P/Q Type Calcium Channel Cav2.1 Defines a Unique Subset of Glomeruli in the Mouse
894 Olfactory Bulb. Frontiers in Cellular Neuroscience *12*, 295.

895 Quinlan, A.R., and Hall, I.M. (2010). BEDTools: a flexible suite of utilities for comparing
896 genomic features. Bioinformatics *26*, 841-842.

897 Rane, C.K., Jackson, S.R., Pastore, C.F., Zhao, G., Weiner, A.I., Patel, N.N., Herbert, D.R.,
898 Cohen, N.A., and Vaughan, A.E. (2019). Development of solitary chemosensory cells in the
899 distal lung after severe influenza injury. Am J Physiol Lung Cell Mol Physiol *316*, L1141-
900 L1149.

901 Richardson, W.H. (1972). Bayesian-Based Iterative Method of Image Restoration*. J Opt Soc
902 Am *62*, 55-59.

903 Sage, D., Donati, L., Soulez, F., Fortun, D., Schmit, G., Seitz, A., Guiet, R., Vonesch, C., and
904 Unser, M. (2017). DeconvolutionLab2: An open-source software for deconvolution microscopy.
905 Methods *115*, 28-41.

906 Saunders, C.J., Christensen, M., Finger, T.E., and Tizzano, M. (2014). Cholinergic
907 neurotransmission links solitary chemosensory cells to nasal inflammation. Proc Natl Acad Sci U
908 S A *111*, 6075-6080.

909 Sayers, C.L., and Elliott, G. (2016). Herpes Simplex Virus 1 Enters Human Keratinocytes by a
910 Nectin-1-Dependent, Rapid Plasma Membrane Fusion Pathway That Functions at Low
911 Temperature. J Virol *90*, 10379-10389.

912 Sekerkova, G., Zheng, L., Loomis, P.A., Changyaleket, B., Whitlon, D.S., Mugnaini, E., and
913 Bartles, J.R. (2004). Espins are multifunctional actin cytoskeletal regulatory proteins in the
914 microvilli of chemosensory and mechanosensory cells. J Neurosci *24*, 5445-5456.

915 Shestakov, A., Jenssen, H., Nordstrom, I., and Eriksson, K. (2012). Lactoferricin but not
916 lactoferrin inhibit herpes simplex virus type 2 infection in mice. Antiviral Res *93*, 340-345.

917 Shivkumar, M., Milho, R., May, J.S., Nicoll, M.P., Efstathiou, S., and Stevenson, P.G. (2013).
918 Herpes simplex virus 1 targets the murine olfactory neuroepithelium for host entry. J Virol *87*,
919 10477-10488.

920 Shukla, N.D., Tiwari, V., and Valyi-Nagy, T. (2012). Nectin-1-specific entry of herpes simplex
921 virus 1 is sufficient for infection of the cornea and viral spread to the trigeminal ganglia. Mol Vis
922 *18*, 2711-2716.

923 Singh, B.K., Hornick, A.L., Krishnamurthy, S., Locke, A.C., Mendoza, C.A., Mateo, M., Miller-
924 Hunt, C.L., Cattaneo, R., and Sinn, P.L. (2015). The Nectin-4/Afadin Protein Complex and
925 Intercellular Membrane Pores Contribute to Rapid Spread of Measles Virus in Primary Human
926 Airway Epithelia. J Virol *89*, 7089-7096.

927 Singh, B.K., Li, N., Mark, A.C., Mateo, M., Cattaneo, R., and Sinn, P.L. (2016). Cell-to-Cell
928 Contact and Nectin-4 Govern Spread of Measles Virus from Primary Human Myeloid Cells to
929 Primary Human Airway Epithelial Cells. J Virol *90*, 6808-6817.

930 Soneson, C., Love, M.I., and Robinson, M.D. (2015). Differential analyses for RNA-seq:
931 transcript-level estimates improve gene-level inferences. F1000Res *4*, 1521.

932 Tizzano, M., Gulbransen, B.D., Vandenbeuch, A., Clapp, T.R., Herman, J.P., Sibhatu, H.M.,
933 Churchill, M.E., Silver, W.L., Kinnamon, S.C., and Finger, T.E. (2010). Nasal chemosensory
934 cells use bitter taste signaling to detect irritants and bacterial signals. Proc Natl Acad Sci U S A
935 *107*, 3210-3215.

936 Ualiyeva, S., Hallen, N., Kanaoka, Y., Ledderose, C., Matsumoto, I., Junger, W.G., Barrett,
937 N.A., and Bankova, L.G. (2020). Airway brush cells generate cysteinyl leukotrienes through the
938 ATP sensor P2Y2. Science Immunology *5*, eaax7224.

939 Valimaa, H., Tenovuo, J., Waris, M., and Hukkanen, V. (2009). Human lactoferrin but not
940 lysozyme neutralizes HSV-1 and inhibits HSV-1 replication and cell-to-cell spread. Virol J *6*, 53.

941 van der Linden, C., Jakob, S., Gupta, P., Dulac, C., and Santoro, S.W. (2018). Sex separation
942 induces differences in the olfactory sensory receptor repertoires of male and female mice. Nat
943 Commun *9*, 5081.

944 Villar, P.S., Delgado, R., Vergara, C., Reyes, J.G., and Bacigalupo, J. (2017). Energy
945 Requirements of Odor Transduction in the Chemosensory Cilia of Olfactory Sensory Neurons
946 Rely on Oxidative Phosphorylation and Glycolytic Processing of Extracellular Glucose. J
947 Neurosci *37*, 5736-5743.

948 von Moltke, J., Ji, M., Liang, H.E., and Locksley, R.M. (2016). Tuft-cell-derived IL-25 regulates
949 an intestinal ILC2-epithelial response circuit. Nature *529*, 221-225.

950 Wu, Y., Ma, L., Duyck, K., Long, C.C., Moran, A., Scheerer, H., Blanck, J., Peak, A., Box, A.,
951 Perera, A.*, et al.* (2018). A Population of Navigator Neurons Is Essential for Olfactory Map
952 Formation during the Critical Period. Neuron *100*, 1066-1082 e1066.

953 Yamaguchi, T., Yamashita, J., Ohmoto, M., Aoude, I., Ogura, T., Luo, W., Bachmanov, A.A.,
954 Lin, W., Matsumoto, I., and Hirota, J. (2014). Skn-1a/Pou2f3 is required for the generation of
955 Trpm5-expressing microvillous cells in the mouse main olfactory epithelium. BMC Neurosci *15*,
956 13.

957 Yamashita, J., Ohmoto, M., Yamaguchi, T., Matsumoto, I., and Hirota, J. (2017). Skn-1a/Pou2f3
958 functions as a master regulator to generate Trpm5-expressing chemosensory cells in mice. PLoS
959 One *12*, e0189340.

960 Yan, C.H., Faraji, F., Prajapati, D.P., Boone, C.E., and DeConde, A.S. (2020a). Association of
961 chemosensory dysfunction and Covid-19 in patients presenting with influenza-like symptoms.
962 Int Forum Allergy Rhinol.

963 Yan, C.H., Faraji, F., Prajapati, D.P., Ostrander, B.T., and DeConde, A.S. (2020b). Self-reported
964 olfactory loss associates with outpatient clinical course in Covid-19. Int Forum Allergy Rhinol.

965 Yang, J., Zhu, X., Liu, J., Ding, X., Han, M., Hu, W., Wang, X., Zhou, Z., and Wang, S. (2012).
966 Inhibition of Hepatitis B virus replication by phospholipid scramblase 1 in vitro and in vivo.
967 Antiviral Res *94*, 9-17.

968 Yu, J., Li, M., Wilkins, J., Ding, S., Swartz, T.H., Esposito, A.M., Zheng, Y.M., Freed, E.O.,
969 Liang, C., Chen, B.K.*, et al.* (2015). IFITM Proteins Restrict HIV-1 Infection by Antagonizing
970 the Envelope Glycoprotein. Cell Rep *13*, 145-156.

971 Zerbino, D.R., Achuthan, P., Akanni, W., Amode, M.R., Barrell, D., Bhai, J., Billis, K.,
972 Cummins, C., Gall, A., Giron, C.G.*, et al.* (2018). Ensembl 2018. Nucleic Acids Res *46*, D754-
973 D761.

974 Zhang, Y., Hoon, M.A., Chandrashekar, J., Mueller, K.L., Cook, B., Wu, D., Zuker, C.S., and
975 Ryba, N.J. (2003). Coding of sweet, bitter, and umami tastes: different receptor cells sharing
976 similar signaling pathways. Cell *112*, 293-301.

977 Zheng, Y., Qin, Z., Ye, Q., Chen, P., Wang, Z., Yan, Q., Luo, Z., Liu, X., Zhou, Y., Xiong, W.,
978 *et al.* (2014). Lactoferrin suppresses the Epstein-Barr virus-induced inflammatory response by
979 interfering with pattern recognition of TLR2 and TLR9. Lab Invest *94*, 1188-1199.

980 Zheng, Y., Zhang, W., Ye, Q., Zhou, Y., Xiong, W., He, W., Deng, M., Zhou, M., Guo, X.,
981 Chen, P., *et al.* (2012). Inhibition of Epstein-Barr virus infection by lactoferrin. J Innate Immun
982 *4*, 387-398.

983 Ziegler, C.G.K., Allon, S.J., Nyquist, S.K., Mbano, I.M., Miao, V.N., Tzouanas, C.N., Cao, Y.,
984 Yousif, A.S., Bals, J., Hauser, B.M., *et al.* (2020). SARS-CoV-2 receptor ACE2 is an interferon-
985 stimulated gene in human airway epithelial cells and is detected in specific cell subsets across
986 tissues. Cell.

987

Figure legends

Figure 1. Fluorescence activated sorting (FACS) of cells isolated from the olfactory epithelium.

a. TRPM5 promoter driven expression of eGFP and OMP promoter driven expression of mCherry in the olfactory epithelium. Expression of eGFP is found both in MVCs that do not express mCherry (asterisk) and in OSNs double labeled with eGFP and mCherry (arrow). **i.** Composite, **ii.** eGFP, **iii.** mCherry, **iv**. Composite magnification. Magenta: mCherry, green: eGFP. Scale bar: i-iii, 50 mm, iv, 10 mm.

b. Schematic of RNA-seq process from tissue to RNA extraction. Mouse OE was dissociated into single cells and sorted via FACS. RNA was extracted from each of the resulting cell populations.

c. Two isolated OSNs differing in eGFP expression. Magenta: mCherry, green: eGFP. Scale bar: 10 mm.

d. Distribution of mCherry and eGFP fluorescence intensity for FACS-sorted cells. Three cell populations were isolated for RNAseq: Cells with low OMP promoter-driven mCherry expression and high TRPM5 promoter-driven eGFP expression (MVC_eGFP cells), cells with high OMP promoter-driven mCherry and low eGFP expression (OSN_eGFP- cells) and cells with eGFP expression of the same magnitude as MVC_eGFP cells and high OMP promoter-driven mCherry expression (OSN_eGFP+ cells). The number of cells collected for this FACS run were: OSN_eGFP-s 1,500,000, OSN_eGFP+s 5336 and MVC_eGFP cells 37,178.

e. qPCR levels (normalized to levels 18s RNA) for expression of transcripts encoding for OMP (**i**), TRPM5 (**ii**), eGFP (**iii**) and ChAT (**iv**). The asterisks denote significant differences tested

1011 with either t-test or ranksum with p-values below the significance p-value corrected for multiple
1012 comparisons using the false discovery rate (pFDR)(Curran-Everett, 2000). pFDR is 0.033 for
1013 OMP, 0.05 for TRPM5, 0.05 for eGFP and 0.03 for ChAT, n=8 for OMP OSN_eGFP-s, 4 for
1014 OMP OSN_eGFP+s and 4 for MVC_eGFP cells.
1015
1016 **Figure 2. Decreased yield of OSN_eGFP+ cells when mice are moved from low ventilation**
1017 **(LV) to high ventilation (HV) cages.**
1018 **a and b.** Distribution of mCherry and eGFP fluorescence intensity for FACS-sorted cells that
1019 either were not transferred to HV cages (**a**) or were transferred to HV cages for 22 days before
1020 sorting (**b**).
1021 **c.** Time course showing change in the number of sorted OSN_eGFP+s after mice were
1022 transferred to HV cages.
1023 **d and e.** Dependence of the yield of OSN_eGFP+ cells after sorting on the number of days in
1024 LV cages (**d**) or the number of days in HV cages (**e**).
1025
1026 **Figure 3. Coverage of TRPM5 transcript by RNAseq in the different cell groups sorted**
1027 **from the olfactory epithelium**
1028 **a.** In situ for TRPM5 and OMP transcripts in the olfactory epithelium shows strong label for
1029 TRPM5 in MVCs (asterisks) and sparse labeling in the OSN nuclear layer (arrows). **i.** OMP, **ii.**
1030 TRPM5, **iii.** Composite. The scale bar is 100 μm.
1031 **b and c.** Coverage of the reads for the TRPM5 transcript for the different cell groups. Read
1032 coverage was computed with 'Samtools depth' over the region corresponding to the Trpm5 gene.

b. Coverage per exon. All samples normalized to TRPM5 reads show distribution among exons with little difference between MVC and OSN_eGFP+ cells.

c. Coverage shown per base pair as a function of location in the genomic DNA. Plots show read depth per base pair for each cell type normalized to total number of mapped reads. Gray shading indicates 95% confidence interval.

Figure 4. RNAseq comparison of OSN_eGFP- and OSN_eGFP+ cells.

a. Heatmap showing the top 10 upregulated and top 10 downregulated genes identified by DESeq2.

b. Heatmap showing all *Olfr* genes detected in the data.

For both a and b, row and column order were determined automatically by the *pHeatmap* package in R. For each data point relative expression was calculated by subtracting the average row value from each individual value.

c. Volcano plot of all Olfactory receptors, demonstrating the small number of enriched olfactory receptors in the OSN_eGFP+ population.

d. Hierarchical clustering of transcripts for taste transduction and transcripts expressed in canonical and non-canonical OSNs identified by RNAseq as significantly different in expression between the cell groups. We compared expression of transcripts involved in taste transduction, canonical olfactory transduction, and non-canonical OSNs. The non-canonical OSNs considered here included guanilyl-cyclase D (GC-D) OSNs (Juilfs et al., 1997), Trpc2 OSNs (Omura and Mombaerts, 2014), Cav2.1 OSNs (Pyrski et al., 2018), and OSNs expressing trace amine-associated receptors (Taars) (Liberles, 2015). Transcripts identified by DESeq2.

e. Gene ontology (GO) term enrichment was calculated from differentially expressed genes using *TopGO* in R. An enrichment value for genes with Fischer p value <0.05 was calculated by dividing the number of expressed genes within the GO term by the number expected genes (by random sampling, determined by *TopGO*).

Figure 5. RNAseq comparison of OSN_eGFP- and OSN_eGFP+ vs. MVC_eGFP cells. **a and b.** Heatmaps showing hierarchical clustering of the top 10 upregulated and top 10 downregulated genes identified by DESeq2. **a.** OSN_eGFP- vs. MVC_eGFP cells. **b**. OSN_eGFP+ vs. MVC_eGFP cells. For both a and b, row and column order were determined automatically by the *pHeatmap* package in R. For each data point relative expression was calculated by subtracting the average row value from each individual value. **c and d.** Gene ontology (GO) term enrichment was calculated from differentially expressed genes using *TopGO* in R. **c.** OSN_eGFP- vs. MVC_eGFP cells. **d**. OSN_eGFP+ vs. MVC_eGFP cells. An enrichment value for genes with Fischer p value <0.05 was calculated by dividing the number of expressed genes within the GO term by the number expected genes (by random sampling, determined by *TopGO*).

Figure 6. Significant differences in virally-related gene ontology. Heatmaps show hierarchical clustering of significantly differentially expressed genes identified by DESeq2. **a.** MVC_eGFP cells compared to OSN_eGFP-. **b.** OSN_eGFP+ compared to OSN_eGFP-.

Figure 7. Intranasal inoculation with HSV-1 elicits a decrease in OSNs.

a and b. Distribution of mCherry and eGFP fluorescence intensity for FAC-sorted cells that either were not infected (**a**) or were inoculated intranasally with 10 µL of solution per naris (20 µL total with HSV-1 (1x 10^6 PFU/naris; McKrae strain) 5 DPI (**b**).

c. Fraction of total cells for OSN_eGFP- (**i**), OSN_eGFP+ (**ii**) or MVC (**iii**) cell groups. GLM analysis yielded significant effects for the fraction of OSN_eGFP- compared to MVCs ($p<0.001$) and for the interaction between the fraction of OSN_eGFP- compared to MVCs and HSV-1 treatment ($p<0.001$, 75 observations, 69 d.f., GLM F-statistic=111 and p-value < 0.001, n=14 mice for control, n=11 mice for HSV-1 inoculation). Asterisks denote a significant difference post-hoc with t-test p-value < pFDR = 0.047.

Name	OSN_eGFP-	OSN_eGFP+	MVC_eGFP	p-value adjusted
Olfr292	3.61	959	4.29	6.35E-09
Olfr282	2.05	486	0	8.01E-05
Olfr1434	53.3	7730	0	9.71E-16
Olfr390	101	10800	43.1	1.56E-16
Olfr305	6.14	612	0	6.3E-12
Olfr293	6.96	664	16.9	1.42E-07
Olfr378	3.41	322	0	1.1E-06
Olfr128	39.6	3660	12.7	7.33E-14
Olfr344	16.2	1050	0	1.4E-11
Olfr307	7.59	393	0	3.76E-06
Olfr391	156	8000	9.79	1.01E-15
Olfr299	13.1	651	0	4.58E-09
Olfr142	36.4	1720	3.77	1.62E-08
Olfr1	147	5720	52.7	3.08E-10
Olfr1279	16.4	552	10.9	3.52E-07
Olfr39	13.8	388	21	2.81E-06
Olfr1447	64.1	1610	0	1.23E-07
Olfr728	2150	45700	320	6.13E-22
Olfr727	560	11000	179	1.64E-07
Olfr1555-ps1	10.1	175	0	0.0397
Olfr346	27.6	465	0	3.85E-05
Olfr1228	533	5320	35.4	3.09E-08
Olfr1181	87.4	766	4.61	0.000766
Olfr943	97.1	844	2.89	0.000886
Olfr298	60.1	509	0	0.00132

Table 1. Levels of expression and adjusted p-value for the olfactory receptor genes whose levels are significantly higher in OSN_eGFP+ compared to OSN_eGFP-. These olfactory receptors had an adjusted p-value for expression level difference between OSN_eGFP+ compared to OSN_eGFP- and had a fold change > 4 and average expression > 100 counts.

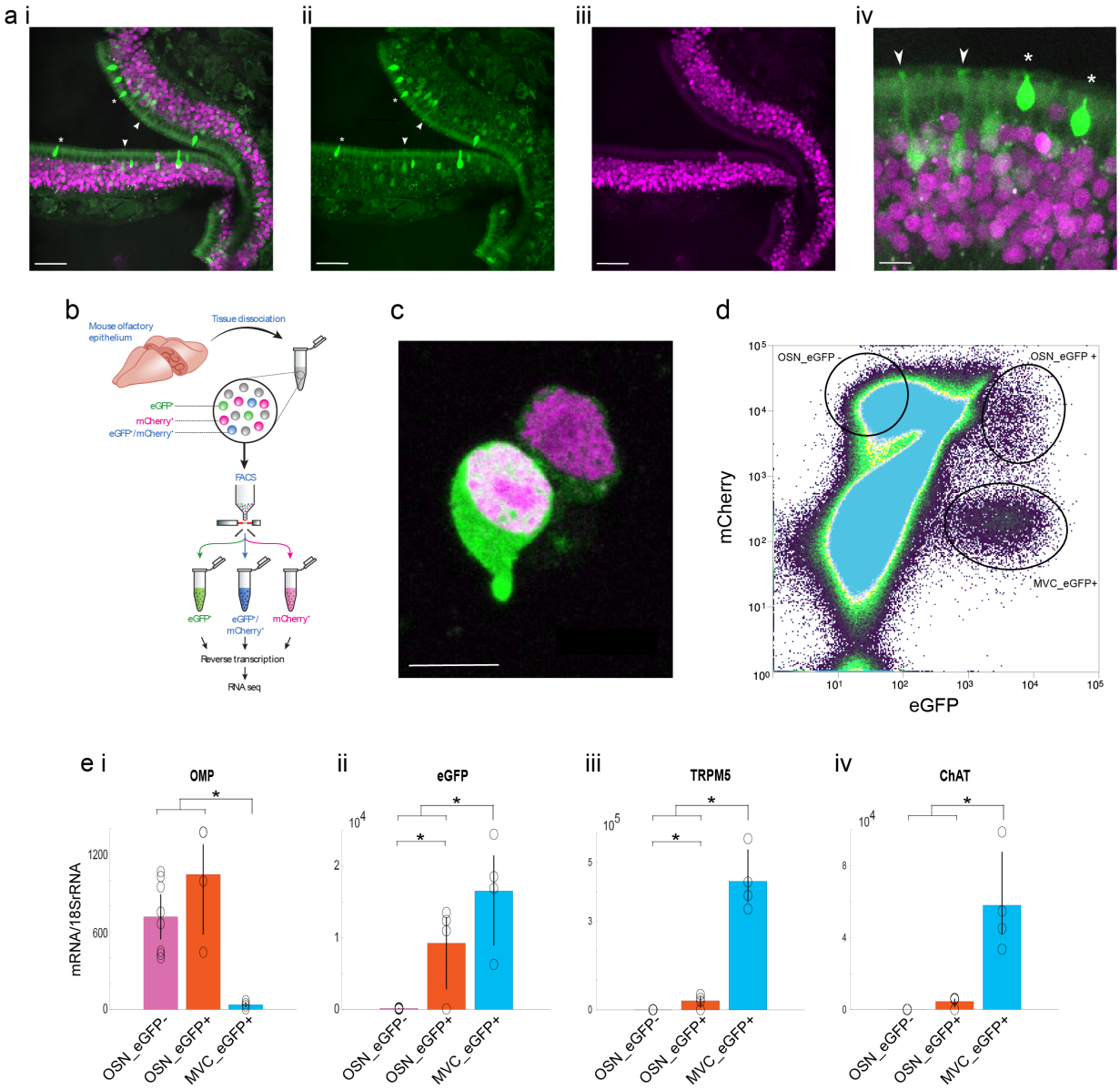

Figure 1. Fluorescence activated sorting (FACS) of cells isolated from the olfactory epithelium.

a. TRPM5 promoter driven expression of eGFP and OMP promoter driven expression of mCherry in the olfactory epithelium. Expression of eGFP is found both in MVCs that do not express mCherry (asterisk) and in OSNs double labeled with eGFP and mCherry (arrow). **i.** Composite, **ii.** eGFP, **iii.** mCherry, **iv**. Composite magnification. Magenta: mCherry, green: eGFP. Scale bar: i-iii, 50 μm, iv, 10 μm.

b. Schematic of RNA-seq process from tissue to RNA extraction. Mouse OE was dissociated into single cells and sorted via FACS. RNA was extracted from each of the resulting cell populations.

c. Two isolated OSNs differing in eGFP expression. Magenta: mCherry, green: eGFP. Scale bar: 10 μm.

d. Distribution of mCherry and eGFP fluorescence intensity for FACS-sorted cells. Three cell populations were isolated for RNAseq: Cells with low OMP promoter-driven mCherry expression and high TRPM5 promoter-driven eGFP expression (MVC_eGFP cells), cells with high OMP promoter-driven mCherry and low eGFP expression (OSN_eGFP- cells) and cells with eGFP expression of the same magnitude as MVC_eGFP cells and high OMP promoter-driven mCherry expression (OSN_eGFP+ cells). The number of cells collected for this FACS run were: OSN_eGFP-s 1,500,000, OSN_eGFP+s 5336 and MVC_eGFP cells 37,178.

e. qPCR levels (normalized to levels 18s RNA) for expression of transcripts encoding for OMP (**i**), TRPM5 (**ii**), eGFP (**iii**) and ChAT (**iv**). The asterisks denote significant differences tested with either t-test or ranksum with p-values below the significance p-value corrected for multiple comparisons using the false discovery rate (pFDR)(Curran-Everett, 2000). pFDR is 0.033 for OMP, 0.05 for TRPM5, 0.05 for eGFP and 0.03 for ChAT, n=8 for OMP OSN_eGFP-s, 4 for OMP OSN_eGFP+s and 4 for MVC_eGFP cells.

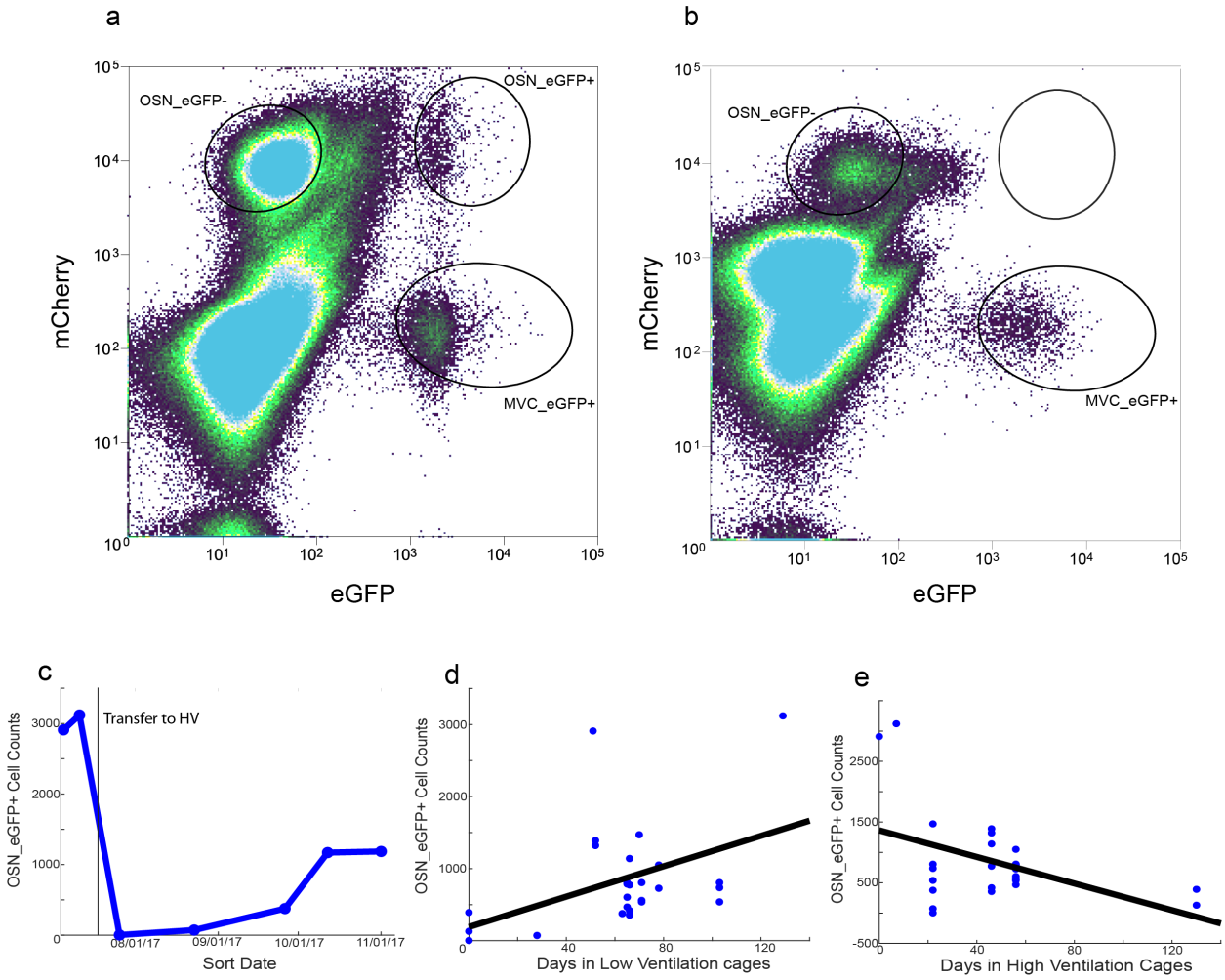

Figure 2. Decreased yield of OSN_eGFP+ cells when mice are moved from low ventilation (LV) to high ventilation (HV) cages.

a and b. Distribution of mCherry and eGFP fluorescence intensity for FACS-sorted cells that either were not transferred to HV cages (**a**) or were transferred to HV cages for 22 days before sorting (**b**).

c. Time course showing change in the number of sorted OSN_eGFP+s after mice were transferred to HV cages.

d and e. Dependence of the yield of OSN_eGFP+ cells after sorting on the number of days in LV cages (**d**) or the number of days in HV cages (**e**).

1134

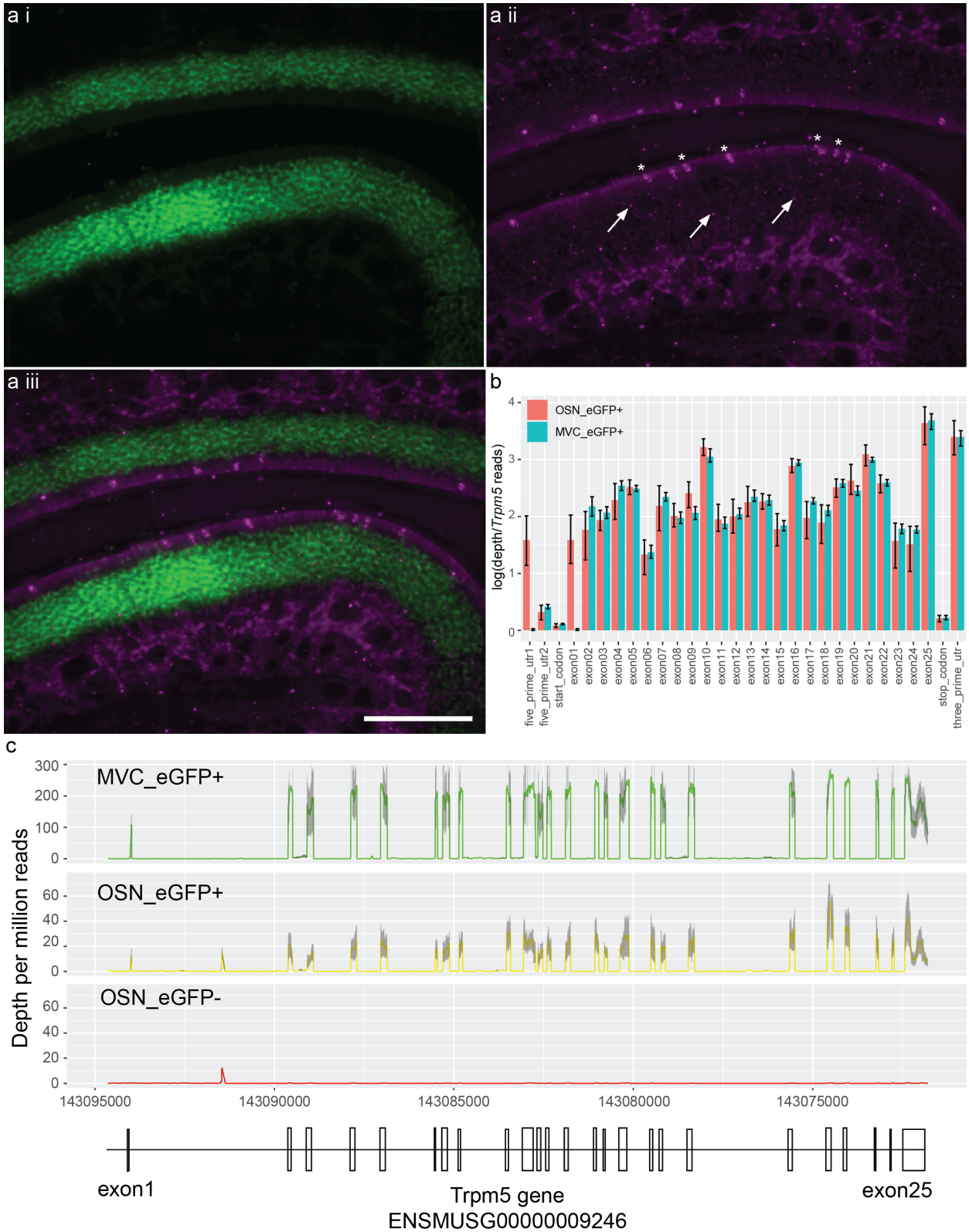

1135

Figure 3. Coverage of TRPM5 transcript by RNAseq in the different cell groups sorted from the olfactory epithelium

a. In situ for TRPM5 and OMP transcripts in the olfactory epithelium shows strong label for TRPM5 in MVCs (asterisks) and sparse labeling in the OSN nuclear layer (arrows). **i.** OMP, **ii.** TRPM5, **iii.** Composite. The scale bar is 100 μm.

b and c. Coverage of the reads for the TRPM5 transcript for the different cell groups. Read coverage was computed with 'Samtools depth' over the region corresponding to the Trpm5 gene.

b. Coverage per exon. All samples normalized to TRPM5 reads show distribution among exons with little difference between MVC and OSN_eGFP+ cells.

c. Coverage shown per base pair as a function of location in the genomic DNA. Plots show read depth per base pair for each cell type normalized to total number of mapped reads. Gray shading indicates 95% confidence interval.

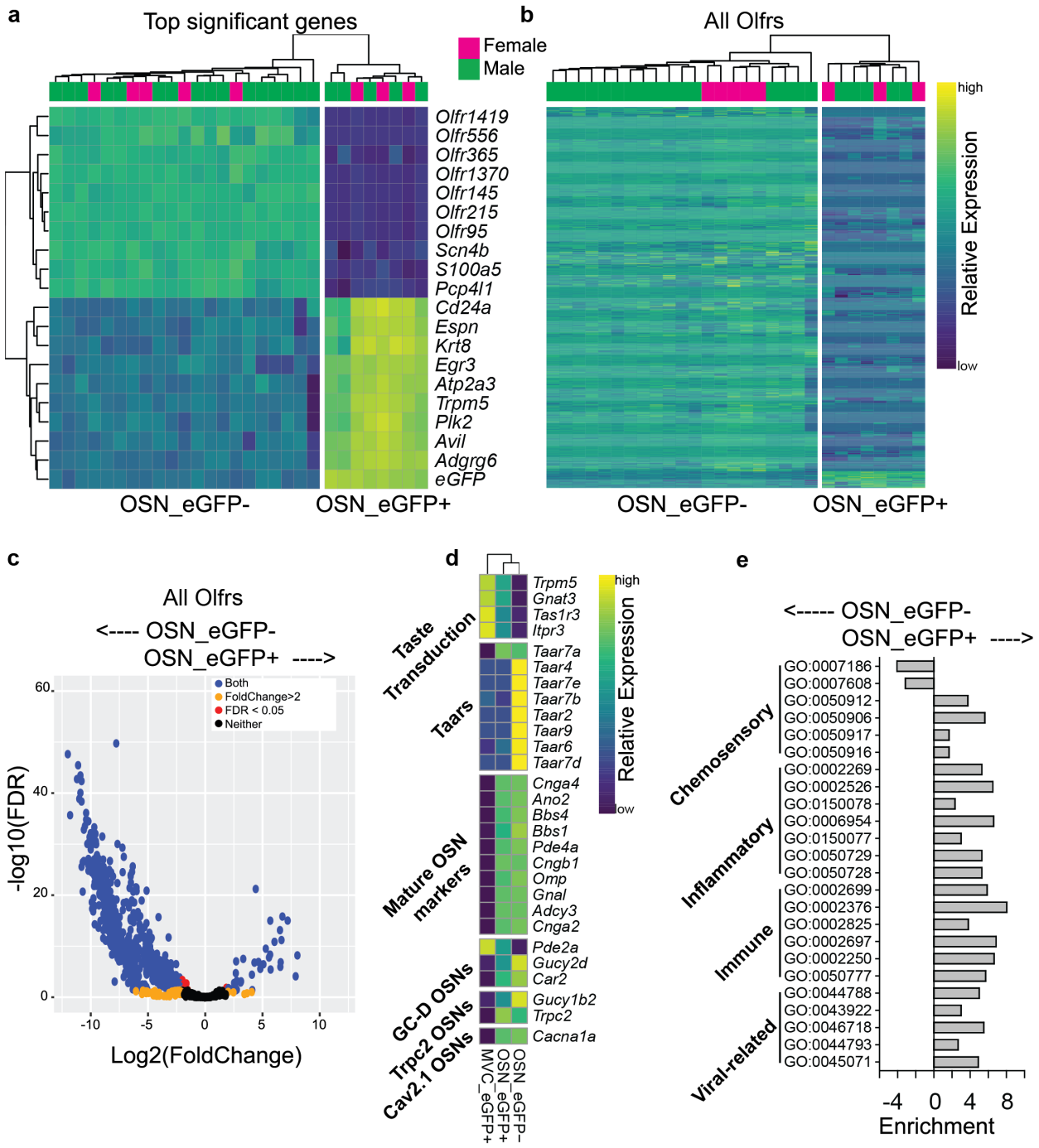

Figure 4. RNAseq comparison of OSN_eGFP- and OSN_eGFP+ cells.

a. Heatmap showing the top 10 upregulated and top 10 downregulated genes identified by DESeq2.

b. Heatmap showing all *Olfr* genes detected in the data.

For both a and b, row and column order were determined automatically by the *pHeatmap* package in R. For each data point relative expression was calculated by subtracting the average row value from each individual value.

c. Volcano plot of all Olfactory receptors, demonstrating the small number of enriched olfactory receptors in the OSN_eGFP+ population.

d. Hierarchical clustering of transcripts for taste transduction and transcripts expressed in canonical and non-canonical OSNs identified by RNAseq as significantly different in expression between the cell groups. We compared expression of transcripts involved in taste transduction, canonical olfactory transduction, and non-canonical OSNs. The non-canonical OSNs considered here included guanilyl-cyclase D (GC-D) OSNs (Juilfs et al., 1997), Trpc2 OSNs (Omura and Mombaerts, 2014), Cav2.1 OSNs (Pyrski et al., 2018), and OSNs expressing trace amine-associated receptors (Taars) (Liberles, 2015). Transcripts identified by DESeq2.

e. Gene ontology (GO) term enrichment was calculated from differentially expressed genes using *TopGO* in R. An enrichment value for genes with Fischer p value <0.05 was calculated by dividing the number of expressed genes within the GO term by the number expected genes (by random sampling, determined by *TopGO*).

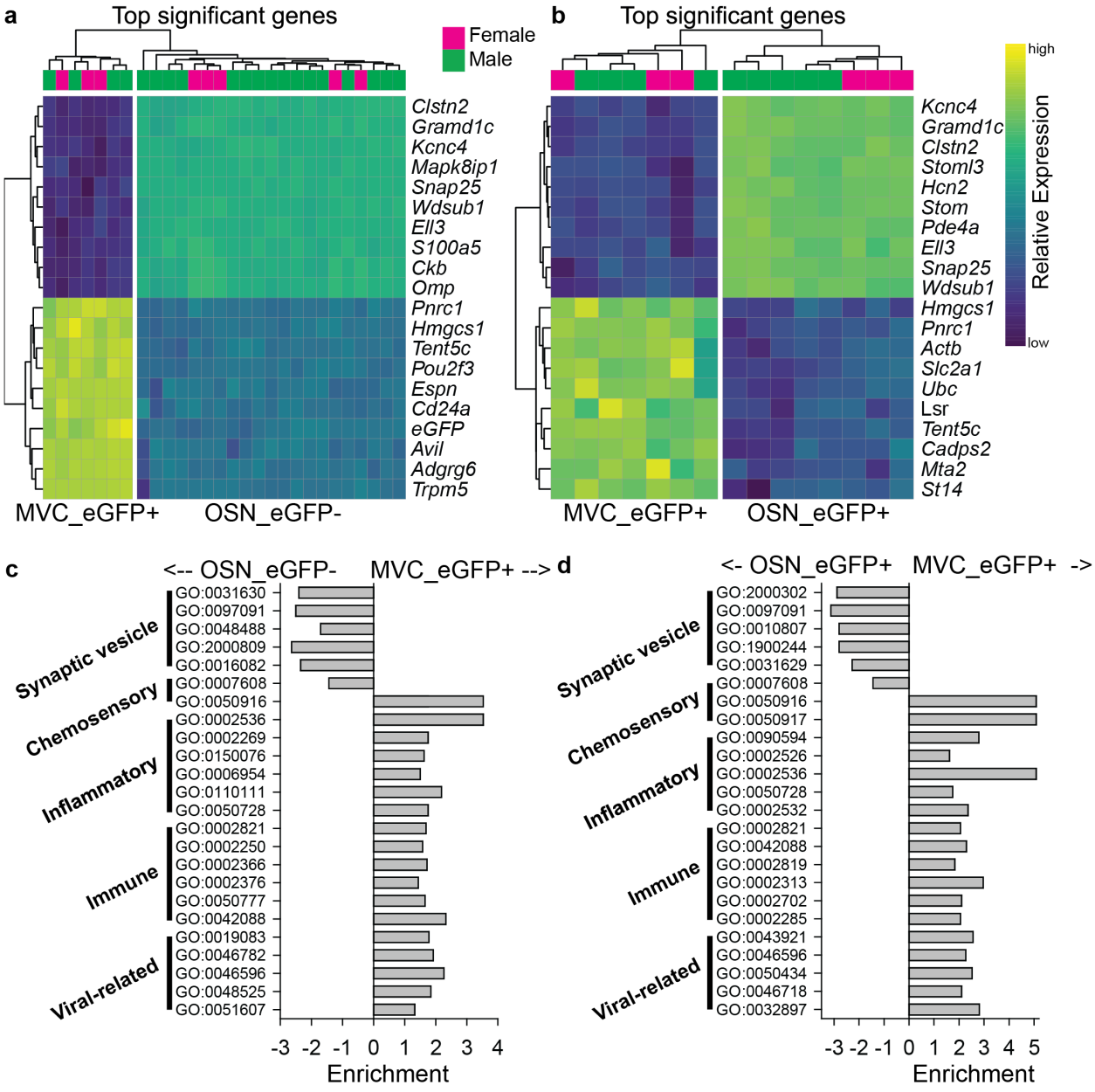

Figure 5. RNAseq comparison of OSN_eGFP- and OSN_eGFP+ vs. MVC_eGFP cells.

a and b. Heatmaps showing hierarchical clustering of the top 10 upregulated and top 10 downregulated genes identified by DESeq2. **a.** OSN_eGFP- vs. MVC_eGFP cells. **b.** OSN_eGFP+ vs. MVC_eGFP cells. For both a and b, row and column order were determined automatically by the *pHeatmap* package in R. For each data point relative expression was calculated by subtracting the average row value from each individual value.

c and d. Gene ontology (GO) term enrichment was calculated from differentially expressed genes using *TopGO* in R. **c.** OSN_eGFP- vs. MVC_eGFP cells. **d**. OSN_eGFP+ vs. MVC_eGFP cells. An enrichment value for genes with Fischer p value <0.05 was calculated by dividing the number of expressed genes within the GO term by the number expected genes (by random sampling, determined by *TopGO*).

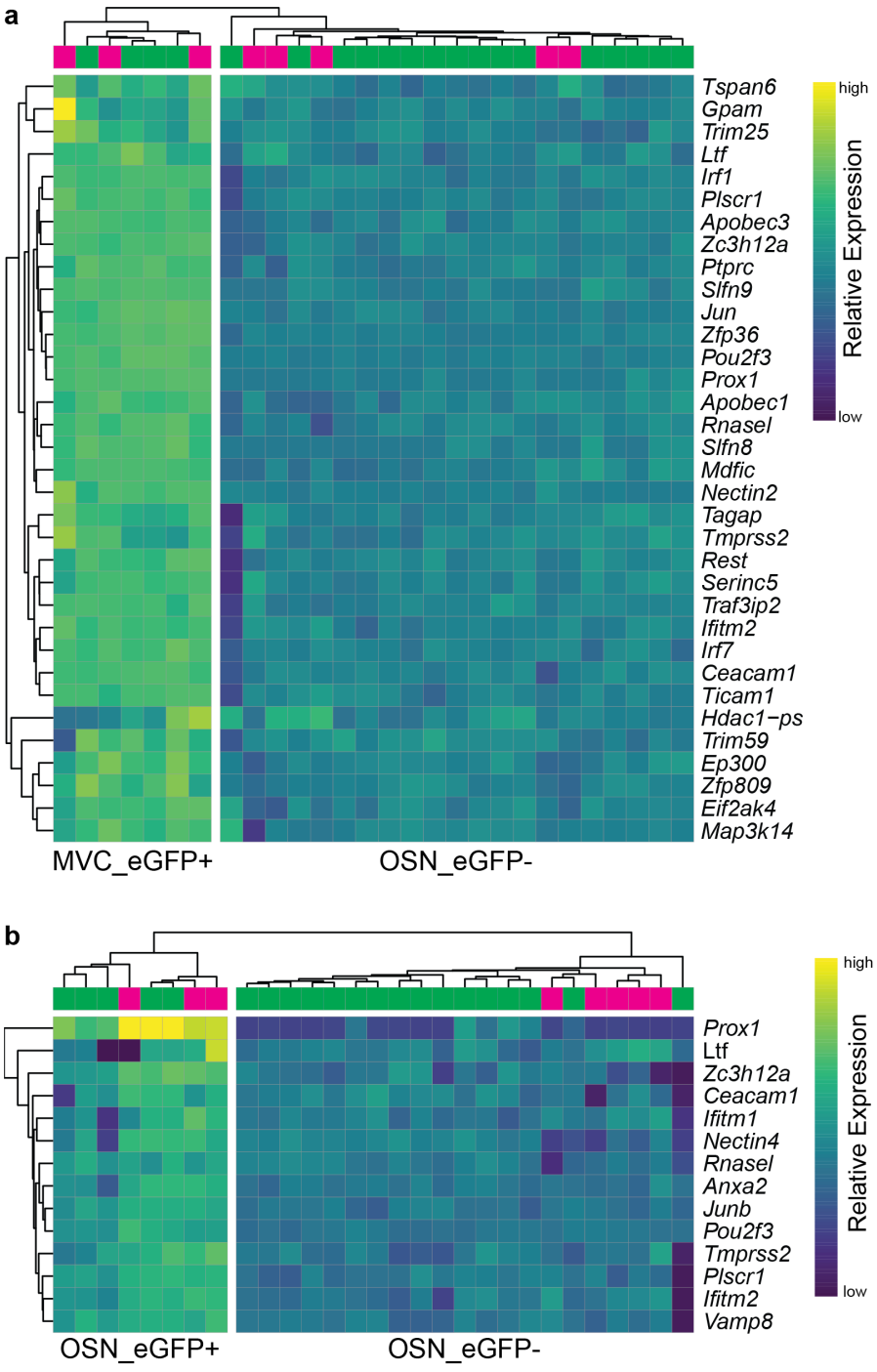

Figure 6. Significant differences in virally-related gene ontology. Heatmaps show hierarchical clustering of significantly differentially expressed genes identified by DESeq2. **a.** MVC_eGFP cells compared to OSN_eGFP-. **b.** OSN_eGFP+ compared to OSN_eGFP-.

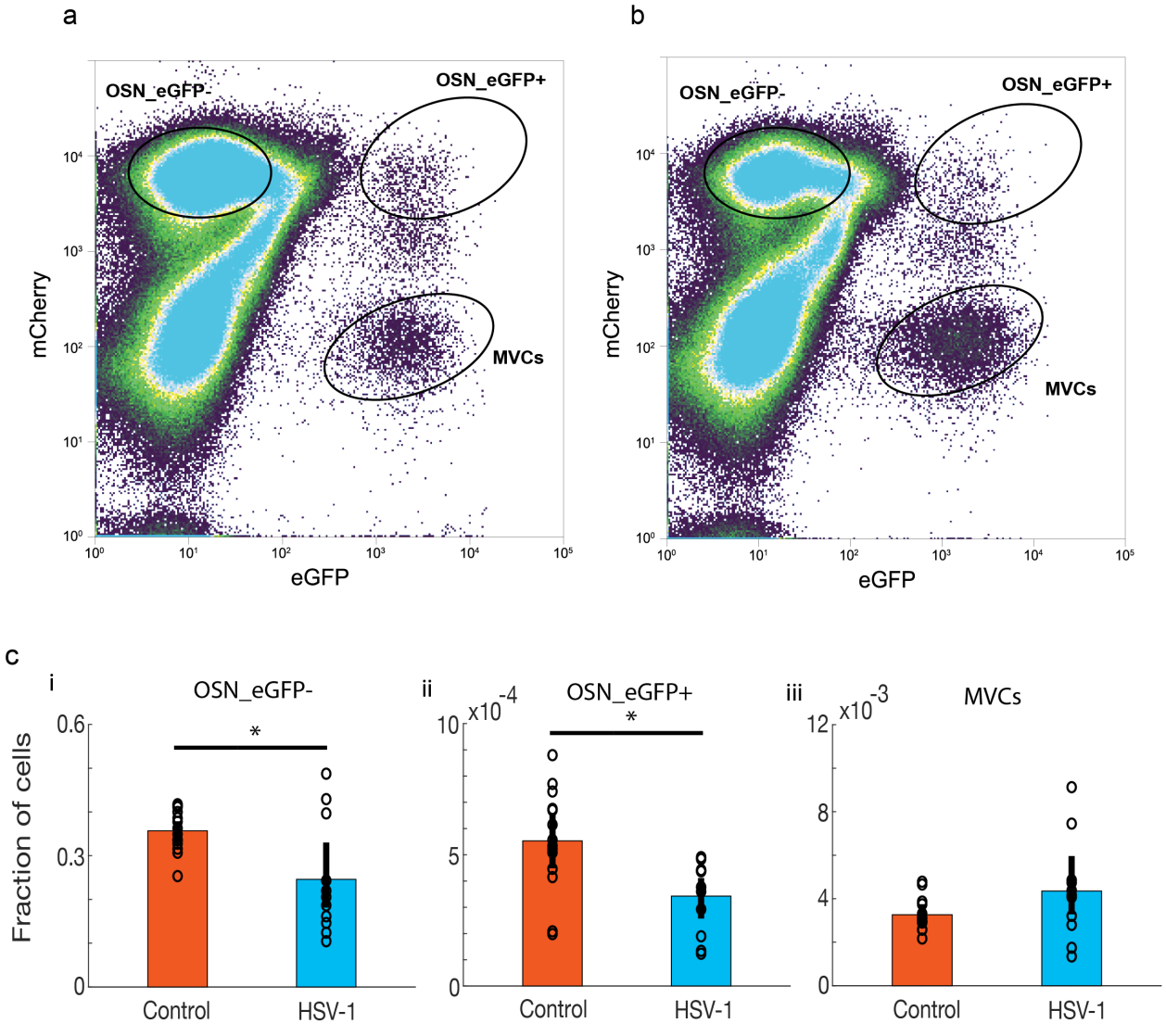

Figure 7. Intranasal inoculation with HSV-1 elicits a decrease in OSNs.

a and b. Distribution of mCherry and eGFP fluorescence intensity for FAC-sorted cells that either were not infected (**a**) or were inoculated intranasally with 10 µL of solution per naris (20 µL total with HSV-1 (1x 10^6 PFU/naris; McKrae strain) 5 DPI (**b**).

c. Fraction of total cells for OSN_eGFP- (**i**), OSN_eGFP+ (**ii**) or MVC (**iii**) cell groups. GLM analysis yielded significant effects for the fraction of OSN_eGFP- compared to MVCs ($p<0.001$) and for the interaction between the fraction of OSN_eGFP- compared to MVCs and HSV-1 treatment ($p<0.001$, 75 observations, 69 d.f., GLM F-statistic=111 and p-value < 0.001, n=14

mice for control, n=11 mice for HSV-1 inoculation). Asterisks denote a significant difference post-hoc with t-test p-value < pFDR = 0.047.

Supplemental Information

Transcriptional profiling reveals TRPM5-expressing cells involved in viral infection in the olfactory epithelium

B. Dnate' Baxter[1,2,‡], Eric D. Larson[3 ‡], Paul Feinstein[4], Arianna Gentile Polese[1,2], Andrew N. Bubak[5], Christy S. Niemeyer[5], Laetitia Merle[1,2], Doug Shepherd[6], Vijay R. Ramakrishnan[3], Maria A. Nagel[5], and Diego Restrepo[1,2,*]

Figure 4 – figure supplement 1. Excel worksheet with the results of comparison of gene transcription between OSN_EGFP+ and OSN_EGFP-.

Figure 4 – figure supplement 2. Metadata for the RNAseq.

Figure 5 - figure supplement 1. Excel worksheet with the results of comparison of gene transcription between MVC_eGFP cells and OSN_EGFP-.

Figure 5 - figure supplement 2. Excel worksheet with the results of comparison of gene transcription between MVC_eGFP cells and OSN_EGFP+.

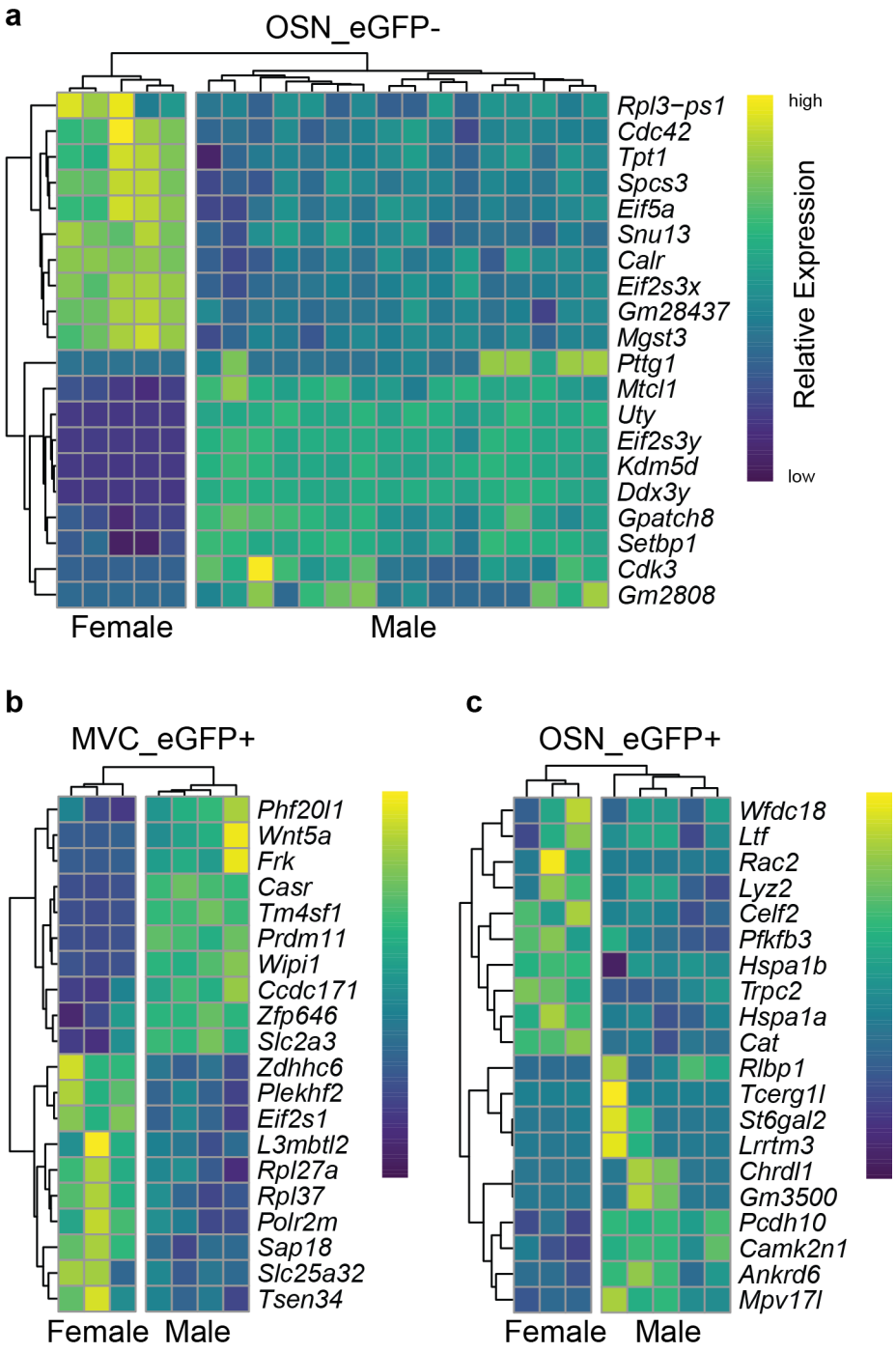

Figure 5 – figure supplement 3. Hierarchical clustering of transcripts identified by RNAseq as significantly differentially expressed between male and female. a. OSN_eGFP-. **b.** MVC_eGFP cells **c.** OSN_eGFP+. Transcripts identified by DESeq2.

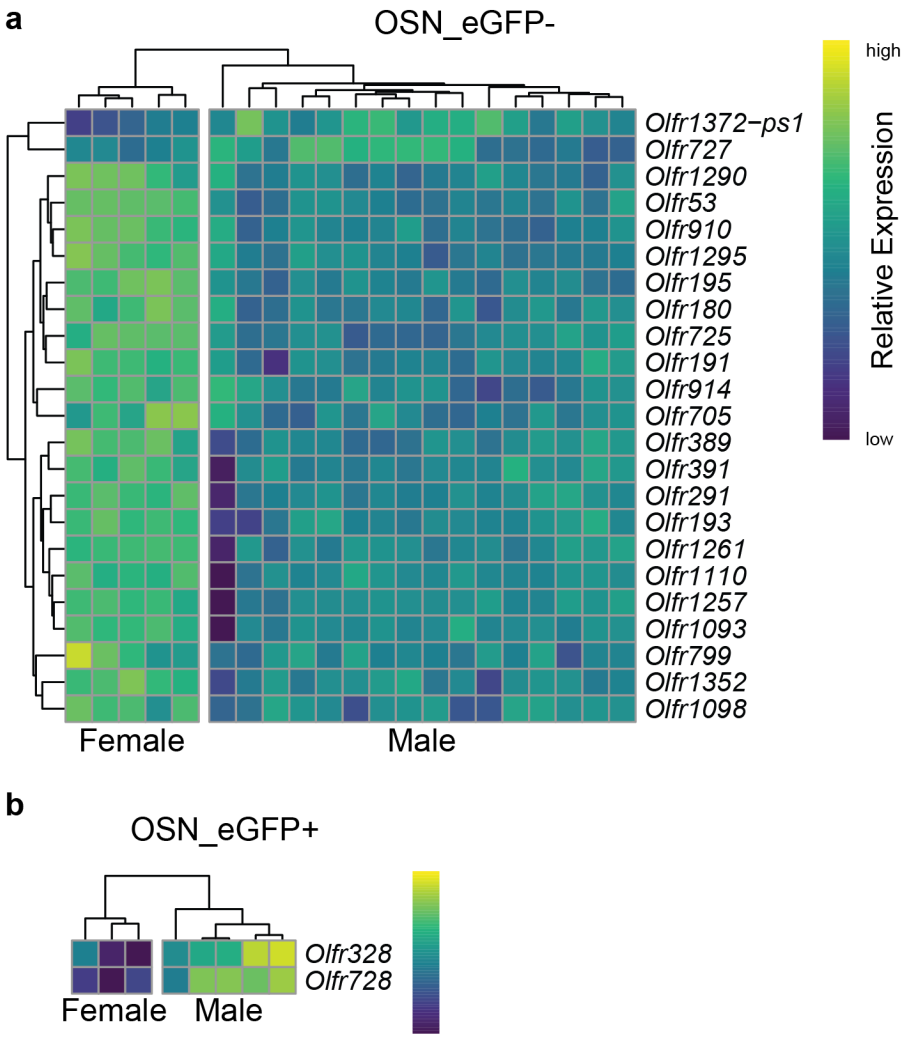

1233

1234 **Figure 5 – figure supplement 4. Hierarchical clustering of olfactory receptor transcripts**

1235 **identified by RNAseq as significantly differentially expressed between male and female. a.**

1236 OSN_eGFP-. **b.** OSN_eGFP+. Transcripts identified by DESeq2.

1237

Figure 6 – figure supplement 1. Excel worksheet with the results of gene ontology enrichment analysis for OSN_eGFP+ compared to OSN_eGFP-.

Figure 6 - figure supplement 2. Excel worksheet with the results of gene ontology enrichment analysis for MVC_eGFP cells compared to OSN_EGFP-.

Figure 6- figure supplement 3. Excel worksheet with the results of gene ontology enrichment analysis for MVC_eGFP cells compared to OSN_EGFP+.

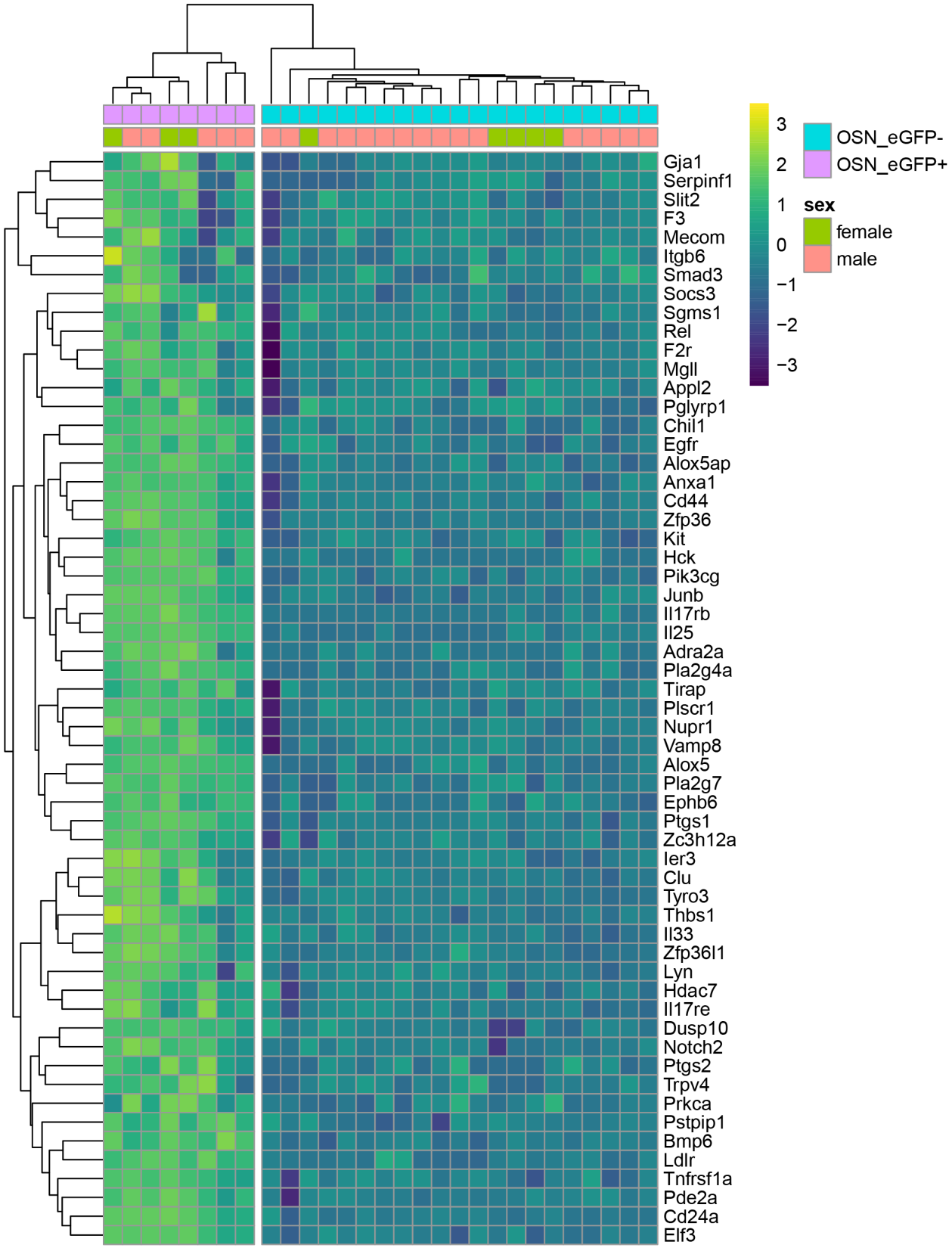

Figure 6- figure supplement 4. Significant differences in inflammation gene ontology for OSN_eGFP+ compared to OSN_eGFP-.

Figure 6- figure supplement 5. Significant differences in inflammation gene ontology for MVC_eGFP+ compared to OSN_eGFP-.

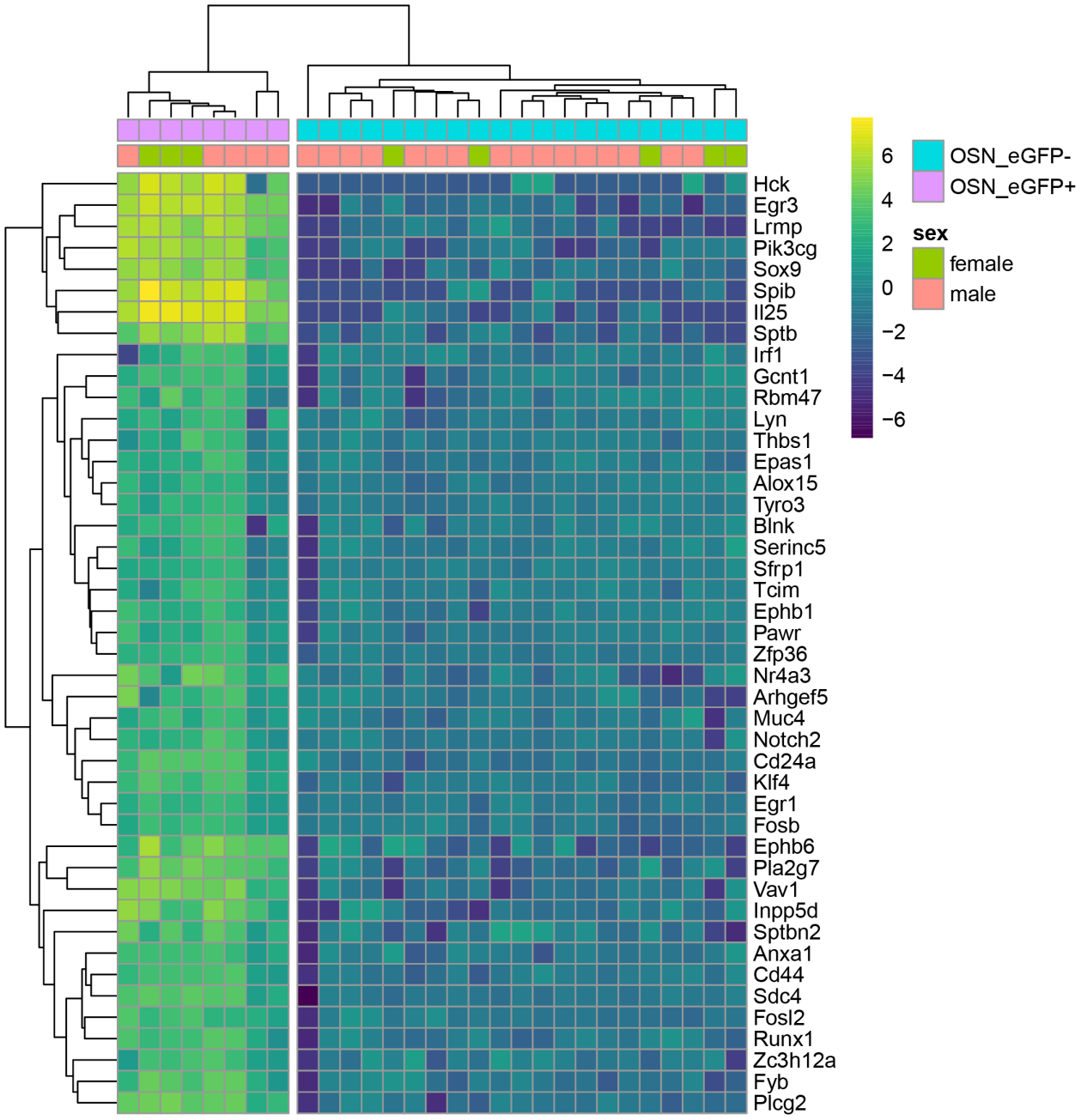

Figure 6- figure supplement 6. Significant differences in immune gene ontology for OSN_eGFP+ compared to OSN_eGFP-.

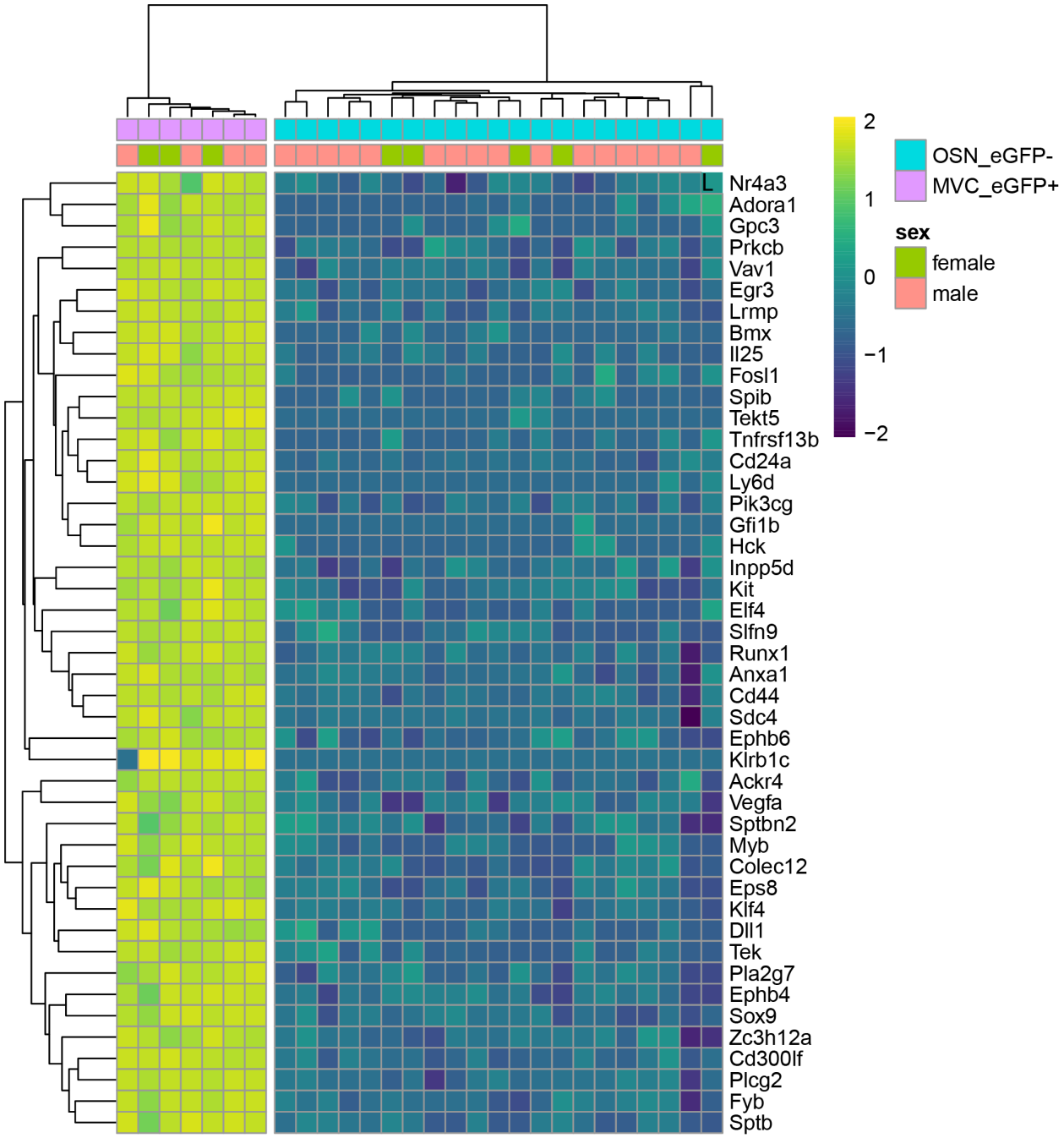

Figure 6- figure supplement 7. Significant differences in immune gene ontology for MVC_eGFP+ compared to OSN_eGFP-.